ORIGINAL ARTICLE

Bistability of the *lac* Operon During Growth of *Escherichia coli* on Lactose and Lactose + Glucose

Atul Narang[a,*], Sergei S. Pilyugin[b]

[a] *Department of Chemical Engineering, University of Florida,*
  Gainesville, FL 32611-6005, USA
[b] *Department of Mathematics, University of Florida, Gainesville, FL 32611-8105, USA*

Abstract The *lac* operon of *Escherichia coli* can exhibit bistability. Early studies showed that bistability occurs during growth on TMG/succinate and lactose + glucose, but not during growth on lactose. More recently, studies with lacGFP-transfected cells show bistability during growth on TMG/succinate, but not during growth on lactose and lactose + glucose. In the literature, these results are invariably attributed to variations in the destabilizing effect of the positive feedback generated by induction. Specifically, during growth on TMG/succinate, *lac* induction generates strong positive feedback because the permease stimulates the accumulation of intracellular TMG, which in turn, promotes the synthesis of even more permease. This positive feedback is attenuated during growth on lactose because hydrolysis of intracellular lactose by β-galactosidase suppresses the stimulatory effect of the permease. It is attenuated even more during growth on lactose + glucose because glucose inhibits the uptake of lactose. But it is clear that the stabilizing effect of dilution also changes dramatically as a function of the medium composition. For instance, during growth on TMG/succinate, the dilution rate of *lac* permease is proportional to its activity, e, because the specific growth rate is independent of e (it is completely determined by the concentration of succinate). However, during growth on lactose, the dilution rate of the permease is proportional to e^2 because the specific growth rate is proportional to the specific lactose uptake rate, which in turn, proportional to e. We show that: (a) This dependence on e^2 creates such a strong stabilizing effect that bistability is virtually impossible during growth on lactose, even in the face of the intense positive feedback generated by induction. (b) This stabilizing effect is weakened during growth on lactose + glucose because the specific growth rate on glucose is independent of e, so that the dilution rate once again contains a term that is proportional to e. These results imply that the *lac* operon is much more prone to bistability if the medium contains carbon sources that cannot be metabolized by the *lac* enzymes, e.g., succinate during growth on TMG/succinate and glucose during growth on lactose + glucose. We discuss the experimental data in the light of these results.

*Corresponding author.
E-mail address:* narang@che.ufl.edu (Atul Narang).

1. Introduction

The *lac* operon has been a topic of considerable interest since the late 1940s. This interest was stimulated by the hope that insights into the mechanism of *lac* induction would shed light on the central problem of development, namely, the mechanism by which genetically identical cells acquire distinct phenotypes (Monod, 1947; Spiegelman, 1948).

Many of the early studies were concerned with the kinetics of enzyme induction. Initial attempts to measure the kinetics were hindered by the fact that lactose, the substrate that stimulates the induction of the *lac* operon, promotes not only the synthesis of the *lac* enzymes, but also their dilution by growth. Under these conditions, it is impossible to separate the kinetics of enzyme synthesis from the masking effects of dilution. This obstacle was overcome by the discovery of *gratuitous inducers*, such as methyl galactoside (MG) and thiomethyl galactoside (TMG). Enzyme synthesis and dilution could be uncoupled by exposing the cells to a medium containing a gratituuous inducer and nongalactosidic carbon sources, such as glucose or/and succinate. The gratuitous inducer promoted enzyme synthesis, but not growth, and the nongalactosidic carbon sources supported growth, but not enzyme synthesis.

Although gratuitous inducers enabled enzyme synthesis and dilution to be uncoupled, an important question remained. Specifically, it was not known whether gratuitous inducers provoked the same enzyme synthesis rate in every cell of a culture. Initial experiments suggested that this was indeed the case. Benzer showed that (Benzer, 1953, Figs. 6 and 7):

1. If noninduced cells of *E. coli* B (pregrown on lactate) were exposed to 1 g/L of lactose, only a small fraction of the cells synthesized β-galactosidase initially. This fraction increased progressively until the culture eventually became homogeneous.
2. In sharp contrast, if noninduced cells were exposed to 2 g/L of MG, all the cells started synthesizing β-galactosidase immediately and at near-maximal rates, i.e., the population became homogeneous almost instantly.

However, it was shown later that the population became homogeneous instantly only because the concentration of the gratuitous inducer was high. At low concentrations of the gratuitious inducer:

1. The population remained heterogeneous for a significant period of time. Furthermore, the smaller the concentration of the gratuitous inducer, the longer the time required for the population to become homogeneous (Cohn and Horibata, 1959a, Table 1).
2. The enzyme synthesis rate was not uniquely determined by the composition of the medium (Fig. 1a). If TMG and glucose were added simultaneously to a culture of *E. coli* ML30 growing on succinate, there was almost no synthesis of β-galactosidase. However, if TMG was added 15 mins before the addition of glucose, β-galactosidase was synthesized for up to 130 generations. Thus, enzyme synthesis is bistable: Preinduced cells remain induced, and noninduced cells remain noninduced.
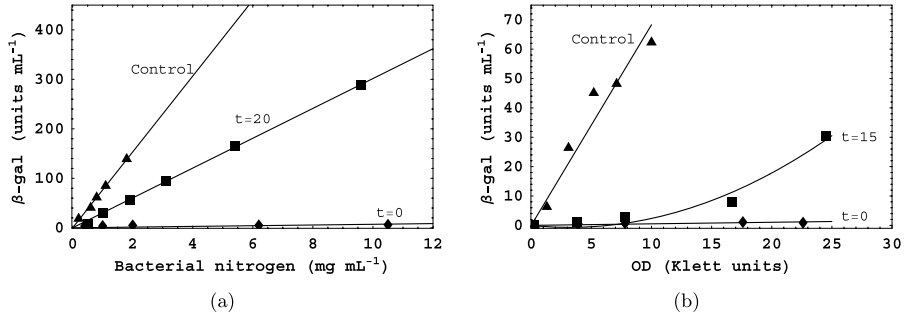
Fig. 1 Bistability during growth of *E. coli* on TMG (Cohn and Horibata, 1959b, Fig. 4) and lactose + glucose (Loomis and Magasanik, 1967, Fig. 3). (a) If glucose and TMG are added simultaneously to a culture growing on succinate, there is no β-galactosidase synthesis (◆). If glucose is added to the culture 20 mins after the addition of TMG, the enzyme is synthesized (■) at a rate that is 50% of the rate observed when only TMG is added to the culture (▲). (b) If lactose is added to a culture growing on glucose, there is no β-galactosidase synthesis (◆). If lactose and glucose are added to the culture after it has been exposed to IPTG for 15 mins, the enzyme synthesis rate (■) increases within a few generation to ∼40% of the rate in a culture exposed to IPTG only (▲).

The existence of bistability and heterogeneity depended crucially upon the existence of *lac* permease (LacY). Both phenomena disappeared in *lacY⁻* (cryptic), but not *lacZ⁻*, mutants (Cohn and Horibata, 1959b).

Subsequent experiments showed that bistability also occurred during growth of *E. coli* K12 3.000 on lactose + glucose (Fig. 1b). If lactose was added to a culture growing on glucose, there was no β-galactosidase synthesis. However, if the culture was exposed to 10^{-3} M IPTG before the addition of lactose, β-galactosidase synthesis persisted for several generations.

These intricate dynamics attracted significant attention among some theoreticians (reviewed in Laurent et al., 2005). In particular, Babloyantz and Sanglier formulated a model of growth on TMG/succinate which took due account of enzyme synthesis by the Jacob–Monod mechanism, and enzyme depletion by degradation (Babloyantz and Sanglier, 1972). They showed that the model yielded the bistability observed in experiments. Chung and Stephanopoulos formulated a similar model, the main differences being that repressor-operator and repressor-inducer binding were assumed to be in quasi-equilibrium, and the enzyme was depleted by both degradation and dilution (Chung and Stephanopoulos, 1996). This model is given by the equations

$$\frac{dx}{dt} = r_s - r_x^- - r_g x, \quad r_s \equiv V_s e \frac{s}{K_s + s}, \ r_x^- \equiv k_x^- x, \tag{1}$$

$$\frac{de}{dt} = r_e^+ - r_e^- - r_g e, \quad r_e^+ \equiv V_e \frac{1 + K_x^2 x^2}{1 + \alpha + K_x^2 x^2}, \ r_e^- \equiv k_e^- e, \tag{2}$$

where x and s denote the intracellular and extracellular TMG concentrations, respectively; e denotes the *lac* permease activity; r_g is the specific growth rate on the nongalactosidic carbon source; r_s, r_x^- denote the specific rates of TMG uptake and expulsion, respectively; and r_e^+, r_e^- denote the specific rates of permease synthesis and degradation, respectively. The expression for r_e^+ is based on the molecular model formulated by Yagil and Yagil,
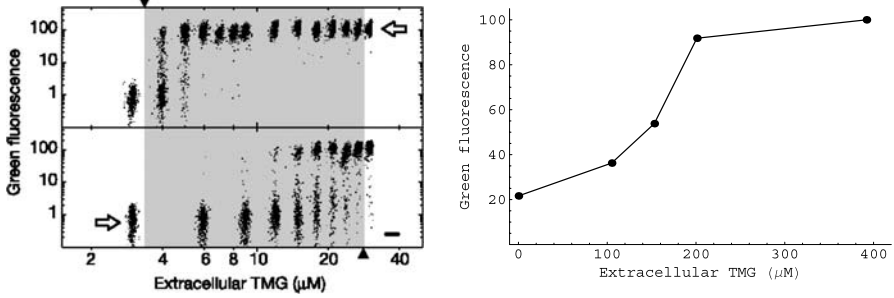
Fig. 2 Dynamics of the *lac* operon (from Ozbudak et al., 2004). (a) Bistability in wild-type cells. The (normalized) green fluorescence provides a measure of the steady state activity of the *lac* operon. The upper (resp., lower) panel shows the green fluorescence observed when an induced (resp., noninduced) inoculum of *Escherichia coli* is grown exponentially on a mixture of succinate and various concentrations of extracellular TMG. Bistability occurs at TMG concentrations between 3 and 30 μM: The green fluorescence is ∼100 if the inoculum is fully induced, and ∼0.5 if the inoculum is noninduced. (b) Monostability in low-repression cells exposed to 1 mM glucose and various concentrations of extracellular TMG.

which assumes that the *lac* operon contains one operator, and the *lac* repressor contains two identical inducer-binding sites (Yagil and Yagil, 1971). The parameter, K_x, is the association constant for the repressor-inducer binding; and α is jointly proportional to the intracellular repressor level and the association constant for repressor-operator binding. Evidently, α is a measure of the *repression*, defined as the ratio, $r_e^+|_{x\to\infty}/r_e^+|_{x=0}$.

Although the experiments done by Cohn and coworkers provided clear evidence of bistability during growth on TMG/succinate, they did not investigate the enzyme levels at a wide variety of conditions. Recently, Ozbudak et al. measured the steady state enzyme levels at various concentrations of TMG (Ozbudak et al., 2004). To this end, they inserted into the chromosome of *Escherichia coli* MG 1655 a reporter *lac* operon, i.e., an operon under the control of the *lac* promoter, which codes for the green fluorescent protein (GFP) instead of the *lac* enzymes. They then exposed non-induced and induced cells to a fixed concentration of succinate, and various concentrations of TMG. It was observed that:

1. When the cells are grown in the presence of succinate and various concentrations of TMG, they exhibit bistability (Fig. 2a). This bistability persists even if glucose is added to the mixture of succinate and TMG.
2. The bistability disappears if the concentration of the *lac* repressor is reduced ∼40-fold by transfecting the cells with the *lac* operator (Fig. 2b).

They also showed that these two observations were mirrored by the bifurcation diagram for the Chung–Stephanopoulos model.

The Yagil and Yagil model of *lac* induction is not consistent with the structure of the *lac* operon and repressor. The *lac* operon contains two auxiliary operators, O_2 and O_3, in addition to the main operator, O_1, and the *lac* repressor contains four inducer-binding sites (Lewis, 2005). Furthermore, these structural features play a crucial role in the formation of DNA loops, the key determinants of *lac* repression (Oehler et al., 1990, 1994) and

induction (Oehler et al., 2006). Molecular models taking due account of the 3 operators and 4 inducer-binding sites yield the *lac* induction rate

$$r_e^+ \equiv V_e \frac{1}{1 + \alpha/(1 + K_x x)^2 + \hat{\alpha}/(1 + K_x x)^4}, \tag{3}$$

where K_x is the association constant for repressor-inducer binding, and $\alpha, \hat{\alpha}$ are related to the *lac* repression stemming from repressor-operator binding and DNA looping, respectively (Kuhlman et al., 2007; Narang, 2007; Santillán et al., 2007). In wild-type *lac*, the repression, $1 + \alpha + \hat{\alpha}$, is 1300, and the bulk of this repression is due to DNA looping ($\alpha \approx 20$, $\hat{\alpha} \approx 1250$) mediated by the interaction of repressor-bound O_1 with O_2 and O_3 (Oehler et al., 1990, 1994). The first goal of this work is to determine if the dynamics of the Chung–Stephanopoulos model are significantly altered by these more realistic kinetics. To this end, we consider the modified Chung–Stephanopoulos model in which the induction rate is replaced by Eq. (3). We show that the dynamics of this modified model are in quantitative agreement with the data.

Ozbudak et al. also studied the growth on lactose and lactose + glucose (Ozbudak et al., 2004, p. 2 of supplement). They found that when noninduced cells (pregrown on succinate) are exposed to various concentrations of lactose and lactose + glucose, the green fluorescence of the cells has a unimodal distribution after 4 hours of growth. They did not report any experiments with induced cells. However, the data for TMG/succinate shows that the green fluorescence of non-induced cells has a bimodal distribution near the upper limit of the bistable region (corresponding to extracellular TMG levels of 15–30 µM in Fig. 2a). The absence of such a bimodal distribution led them to conclude that bistability does not occur during growth on lactose and lactose + glucose. This is consistent with the data obtained by Benzer, but contradicts the data shown in Fig. 1b. The second goal of this work is to seek an explanation for the absence of bistability during growth on lactose, and the conflicting results for lactose + glucose.

The foregoing experimental results have spurred the development of several mathematical models, most of which are concerned with the disappearance of bistability during growth on lactose. Thus far, two mechanisms have been proposed.

The first mechanism proposes that during growth on lactose, there is bistability but it is not observed because the induced cells outgrow the non-induced cells. It seems unlikely that this mechanism, by itself, can explain the data. To see this, suppose that the noninduced inoculum used in the experiments contains 10% induced cells, which double every hour. As a worst-case scenario, assume that the noninduced cells do not grow at all. Then, after 4 h, almost 40% of the population is still noninduced, which is far from the unimodal distribution observed in the experiments.

The second mechanism proposes that bistability does not even exist because positive feedback is suppressed during growth on lactose or lactose + glucose (van Hoek and Hogeweg, 2006; Mahaffy and Savev, 1999; Santillán et al., 2007; Savageau, 2001). More precisely, during growth on TMG/succinate, bistability is feasible because of strong positive feedback: The permease stimulates the accumulation of intracellular TMG, which in turn promotes the synthesis of even more permease (Fig. 3a). The destabilizing effect of this positive feedback produces bistability by overcoming the stabilizing effect of dilution. During growth on lactose, the positive feedback is suppressed because hydrolysis of lactose by β-galactosidase attenuates the stimulatory effect of the permease (Fig. 3b).
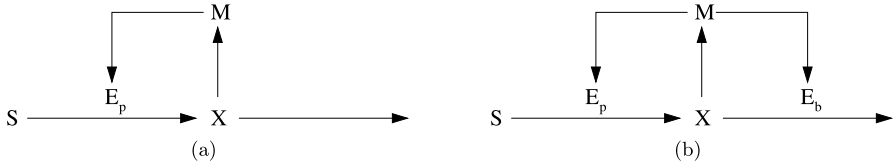
Fig. 3 The dynamics of the inducer are different during growth on (a) TMG/succinate and (b) lactose (adapted from Savageau, 2001). Here, S denotes extracellular TMG or lactose; X denotes intracellular TMG or lactose; M denotes *lac* mRNA; and E_p, E_b denote *lac* permease and β-galactosidase, respectively. (a) Intracellular TMG is discharged from the cell by inducer expulsion, a process that is independent of *lac* enzymes. (b) Intracellular lactose is metabolized by β-galactosidase (E_b).

It is attenuated even more during growth on lactose + glucose because in the presence of glucose, enzyme IIA$^{\text{glc}}$ is dephosphorylated, and inhibits the permease by binding to it (Santillán et al., 2007).

In all these models, the differences in the dynamics of growth on TMG/succinate, lactose, and lactose + glucose are attributed entirely to changes in the destabilizing effect of positive feedback generated by induction. Here, we show that the stabilizing effect of dilution also changes dramatically with the medium composition, and this has equally profound effects on the dynamics of the *lac* operon. Specifically:

1. The stabilizing effect of dilution is much stronger during growth on lactose (as opposed to growth on TMG/succinate). Indeed, during growth on TMG/succinate, the dilution rate of the *lac* enzymes is proportional to their level, e, because the specific growth rate does not depend on the activity of these enzymes—it is completely determined by the concentration of succinate. However, during growth on lactose, the dilution rate is proportional to e^2 because the specific growth rate is proportional to the lactose uptake rate, which in turn, is proportional to the activity of *lac* permease. We show that this stronger stabilizing effect of dilution suppresses bistability on lactose even in the presence of the intense positive feedback.

2. The enhanced stabilizing effect of dilution is attenuated once again during growth on lactose + glucose. This is because the specific growth rate on glucose, a nongalactosidic carbon source like succinate, is independent of e. Thus, in the presence of glucose, the dilution rate once again contains a term that is proportional to e, and the dynamics become similar to those on TMG/succinate, i.e., bistability is feasible provided the positive feedback is sufficiently large.

These results imply that the *lac* operon is much more susceptible to bistability in the presence of nongalactosidic carbon sources, since they serve to suppress the stabilizing effect of dilution.

2. The model

Figure 4 shows the kinetic scheme of the model. Here, S_1, S_2 denote the exogenous lactose (or TMG) and glucose, respectively; E_1, E_2 denote the transport enzymes for lactose (or TMG) and glucose, respectively; X_1, X_2 denote internalized lactose (or TMG) and glucose, respectively; G denotes the GFP synthesized by the reporter *lac* operon; and C^-
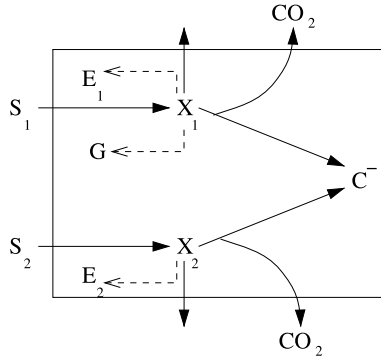
Fig. 4 Kinetic scheme of the model.

denotes all intracellular components except E_i, X_i, and G (thus, it includes precursors, free amino acids, and macromolecules). We assume that:

1. The concentrations of the intracellular components, denoted e_i, x_i, g, and c^-, are based on the dry weight of the cells (g per g dry weight of cells, i.e., g gdw^{-1}). The concentrations of the exogenous substrate and cells, denoted s_i and c, are based on the volume of the reactor (g/L and gdw/L, respectively). The rates of all the processes are based on the dry weight of the cells (g gdw^{-1} h^{-1}). We shall use the term *specific rate* to emphasize this point. The choice of these units implies that if the concentration of any intracellular component, Z, is z g gdw^{-1}, then the evolution of z in batch cultures is given by

$$\frac{dz}{dt} = r_z^+ - r_z^- - \left(\frac{1}{c}\frac{dc}{dt}\right)z,$$

   where r_z^+ and r_z^- denote the specific rates of synthesis and degradation of Z in g gdw^{-1} h^{-1}.
2. The specific uptake rate of S_i, denoted $r_{s,i}$, follows the modified Michaelis–Menten kinetics, $r_{s,i} \equiv V_{s,i} e_i s_i / (K_{s,i} + s_i)$.
3. In the case of glucose or lactose, part of the internalized substrate, denoted X_i, is expelled into the environment. The remainder is converted to C^-, and oxidized to CO_2 for generating energy.
   (a) The specific rate of expulsion of X_i follows first-order kinetics, i.e., $r_{x,i}^- \equiv k_{x,i}^- x_i$.
   (b) The conversion of X_i to C^- and CO_2 also follows first-order kinetics, i.e., $r_{x,i}^+ \equiv k_{x,i}^+ x_i$.
   (c) The specific rate of synthesis of C^- from X_i is $Y_i r_{x,i}^+$, where Y_i is a constant (which will turn out later to be effectively equal to the yield of biomass on S_i).
4. Internalized TMG is completely expelled—it does not support biosynthesis or respiration.
5. The internalized substrates induce the synthesis of the enzymes and GFP.
   (a) The specific synthesis rate of the lactose enzymes, E_1, follows the kinetics

$$r_{e,1} \equiv V_{e,1} \frac{1}{1 + \alpha_1/(1 + K_{x,1}x_1)^2 + \hat{\alpha}_1/(1 + K_{x,1}x_1)^4}, \tag{4}$$

where $K_{x,1}$ is the association constant for repressor-inducer binding, and $\alpha_1, \hat{\alpha}_1$ characterize the transcriptional repression due to repressor-operator binding and DNA looping, respectively. Both α_1 and $\hat{\alpha}_1$ are proportional to the intracellular repressor level (Narang, 2007).

In wild-type cells, $\alpha_1 = 20, \hat{\alpha}_1 = 1250$ (Oehler et al., 1990, Fig. 2). In cells transfected with the *lac* operator, the repressor levels decrease 43-fold (Ozbudak et al., 2004); hence, $\alpha_1 \approx 0, \hat{\alpha}_1 \approx 30$.

(b) The specific synthesis rate of GFP follows the same kinetics as the *lac* operon, i.e.,

$$r_{\text{GFP}} \equiv V_{\text{GFP}} \frac{1}{1 + \alpha_G/(1 + K_{x,1}x_1)^2 + \hat{\alpha}_G/(1 + K_{x,1}x_1)^4}.$$

We shall assume that the promoters of the reporter and native *lac* operons are identical, so that $V_{\text{GFP}} = V_{e,1}$ and $\alpha_G = \alpha_1 = 20$. However, $\hat{\alpha}_G < \hat{\alpha}_1$ because the reporter *lac* operon lacks the auxiliary operator, O_2, which precludes the formation of DNA loops due to interaction between O_1 and O_2. Ozbudak et al. found the repression of the *lac* reporter, $1 + \alpha_G + \hat{\alpha}_G$ to be 170 (Ozbudak et al., 2004), which implies that $\hat{\alpha}_G \approx 150$. If the cells are transfected with the *lac* operator, $\alpha_G \approx 0$, $\hat{\alpha}_G = 4$.

(c) The induction of the glucose enzymes, E_2, is thought to occur by a mechanism similar to the one that induces the *lac* operon (Plumbridge, 2003). Specifically, in the absence of glucose, transcription of the *ptsG* operon is blocked because the repressor (Mlc) is bound to the operator. In the presence of glucose, the enzyme IIBC$^{\text{glc}}$ sequesters Mlc from the operator by an unknown mechanism, thus liberating the operon for transcription. We assume that the specific synthesis rate of E_2 has the form

$$r_{e,2} \equiv V_{e,2} \frac{1}{1 + \alpha_2/(1 + K_{x,2}x_2)},$$

where $K_{x,2}$ and α_2 are phenomenological parameters, i.e., they cannot be expressed in terms of parameters characterizing the molecular interactions.

The data shows that the PTS level in cells growing exponentially on glucose is roughly 5 times the level observed in cells growing exponentially on glycerol (Fig. 5). This implies that $\alpha_2 \approx 4$.

(d) The synthesis of the enzymes and GFP occurs at the expense of the biosynthetic constituents, C^-.

(e) Enzyme and GFP degradation are negligibly small.

(f) Nonspecific diffusion of the substrates into the cell is negligibly small. This is valid for lactose and glucose at the concentrations typically used in the experiments. It is valid for gratuitous inducers, such as TMG, only if the extracellular concentration is <50 μM (Herzenberg, 1959, Fig. 4).

In what follows, we begin by deriving the equations for growth on TMG plus nongalactosidic substrates. We then derive the equations for growth on lactose + glucose, from which the equations for growth on lactose are obtained by letting the concentration of glucose be zero.
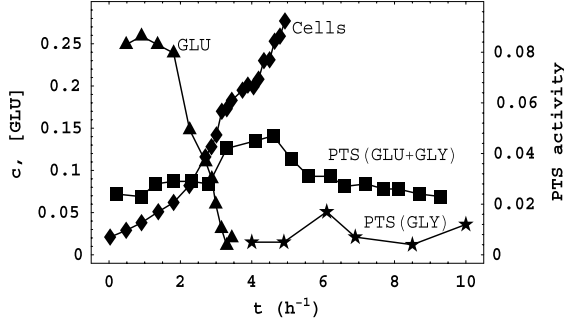
Fig. 5 The phosphotransferase system of enzymes is inducible (Bettenbrock et al., 2006). The concentrations of cells (♦) and glucose (▲) correspond to the growth of *E. coli* on glucose + glycerol. During the first phase of diauxic growth on glucose + glycerol, the PTS activity (■) increases to ∼0.05. During batch growth on pure glycerol, the PTS activity (★) is ∼0.01.

2.1. *Growth in the presence of TMG and non-galactosidic carbon sources*

During growth in the presence of TMG and nongalactosidic carbon sources, the mass balances yield

$$\frac{ds_1}{dt} = -\left[V_{s,1}e_1\frac{s_1}{K_{s,1}+s_1} - k^-_{x,1}x_1\right]c,$$

$$\frac{dx_1}{dt} = V_{s,1}e_1\frac{s_1}{K_{s,1}+s_1} - k^-_{x,1}x_1 - \left(\frac{1}{c}\frac{dc}{dt}\right)x_1,$$

$$\frac{de_1}{dt} = V_{e,1}\frac{1}{1+\alpha_1/(1+K_{x,1}x_1)^2+\hat{\alpha}_1/(1+K_{x,1}x_1)^4} - \left(\frac{1}{c}\frac{dc}{dt}\right)e_1,$$

$$\frac{dg}{dt} = V_{e,1}\frac{1}{1+\alpha_1/(1+K_{x,1}x_1)^2+\hat{\alpha}_G/(1+K_{x,1}x_1)^4} - \left(\frac{1}{c}\frac{dc}{dt}\right)g,$$

$$\frac{dc}{dt} = r_g c$$

where r_g, the exponential growth rate on the nongalactosidic carbon sources, is a fixed parameter (independent of the model variables, s_1, x_1, e_1, g, c). It is completely determined by the concentration of the nongalactosidic carbon sources(s).

It turns out that the dynamics of the experiments can be described by only 2 differential equations. Indeed, since the cell density remains vanishingly small throughout the experiment, there is almost no depletion of extracellular TMG, and s_1 remains essentially equal to its initial value, $s_{1,0}$. Moreover, since $k^-_{x,1} \sim 1$ min^{-1} (Kepes, 1960, Table 1) and $r_g \sim 0.5$ hr^{-1}, x_1 attains quasi-steady state on a time scale of minutes. It follows that the dynamics of E_1 after the first few minutes are well approximated by the equations

$$\frac{de_1}{dt} = V_{e,1}\frac{1}{1+\alpha_1/(1+K_{x,1}x_1)^2+\hat{\alpha}_1/(1+K_{x,1}x_1)^4} - r_g e_1, \tag{5}$$

$$\frac{dg}{dt} = V_{e,1} \frac{1}{1 + \alpha_1/(1 + K_{x,1}x_1)^2 + \hat{\alpha}_G/(1 + K_{x,1}x_1)^4} - r_g g, \tag{6}$$

$$x_1 \approx \frac{V_{s,1}}{k_{x,1}^-} e_1 \sigma_1, \quad \sigma_1 \equiv \frac{s_{1,0}}{K_{s,1} + s_{1,0}}, \tag{7}$$

where (7) shows the quasi-steady state concentration of intracellular TMG.

Equations (5), (6) imply that the maximum steady state level of E_1 and G is $V_{e,1}/r_g$. It is, therefore, natural to define the dimensionless variables

$$\epsilon_1 \equiv \frac{e_1}{V_{e,1}/r_g}, \qquad \gamma \equiv \frac{g}{V_{e,1}/r_g}, \qquad \chi_1 \equiv K_{x,1}x_1, \qquad \tau \equiv r_g t.$$

This yields the dimensionless equations

$$\frac{d\epsilon_1}{d\tau} = \frac{1}{1 + \alpha_1/(1 + \chi_1)^2 + \hat{\alpha}_1/(1 + \chi_1)^4} - \epsilon_1, \tag{8}$$

$$\frac{d\gamma}{d\tau} = \frac{1}{1 + \alpha_1/(1 + \chi_1)^2 + \hat{\alpha}_G/(1 + \chi_1)^4} - \gamma, \tag{9}$$

$$\chi_1 = \bar{\delta}_1 \epsilon_1 \tag{10}$$

where

$$\bar{\delta}_1 \equiv \bar{\delta}_{1,m} \sigma_1, \quad \bar{\delta}_{1,m} \equiv \frac{V_{s,1}(V_{e,1}/r_g)/k_{x,1}^-}{K_{x,1}^{-1}}. \tag{11}$$

It follows from (10), (11) that $\bar{\delta}_{1,m}$ is a measure of the quasi-steady state intracellular TMG concentration at saturating levels of extracellular TMG (measured in units of $K_{x,1}^{-1}$, the dissociation constant for repressor-inducer binding). We can also view $\bar{\delta}_{1,m}$ as a measure of the strength of the positive feedback: Given any σ_1, the strength of the positive feedback, $\partial r_{e,1}/\partial \epsilon_1$, is an increasing function of $\bar{\delta}_{1,m}$. The parameter, $\bar{\delta}_1$, is a measure of the intracellular TMG concentration at any given extracellular TMG level. For a given cell type and nongalactosidic carbon source, $\bar{\delta}_1$ is proportional to σ_1, and hence, can be treated as a surrogate for the extracellular TMG concentration.

2.2. Growth on lactose or lactose + glucose

During growth in the presence of lactose and glucose, the mass balances yield

$$\frac{ds_i}{dt} = -\left(V_{s,i} e_i \frac{s_i}{K_{s,i} + s_i} - k_x^- x_i\right) c, \tag{12}$$

$$\frac{dx_i}{dt} = V_{s,i} e_i \frac{s_i}{K_{s,i} + s_i} - k_{x,i}^- x_i - k_{x,i}^+ x_i - \left(\frac{1}{c}\frac{dc}{dt}\right) x_i, \tag{13}$$

$$\frac{de_1}{dt} = V_{e,1} \frac{1}{1 + \alpha_1/(1 + K_{x,1}x_1)^2 + \hat{\alpha}_1/(1 + K_{x,1}x_1)^4} - \left(\frac{1}{c}\frac{dc}{dt}\right) e_1, \tag{14}$$

$$\frac{dg}{dt} = V_{e,1} \frac{1}{1 + \alpha_1/(1 + K_{x,1}x_1)^2 + \hat{\alpha}_G/(1 + K_{x,1}x_1)^4} - \left(\frac{1}{c}\frac{dc}{dt}\right) g, \tag{15}$$

$$\frac{de_2}{dt} = V_{e,2} \frac{1}{1 + \alpha_2/(1 + K_{x,2}x_2)} - \left(\frac{1}{c}\frac{dc}{dt}\right)e_2, \tag{16}$$

$$\frac{dc^-}{dt} = \sum_{i=1}^{2} (Y_i k_{x,i}^+ x_i) - r_{e,1} - r_{GFP} - r_{e,2} - \left(\frac{1}{c}\frac{dc}{dt}\right)c^-. \tag{17}$$

It is shown in Appendix A that under the experimental conditions, the dynamics of the enzymes and GFP are well approximated by the equations

$$\frac{de_1}{dt} = V_{e,1} \frac{1}{1 + \alpha_1/(1 + K_{x,1}x_1)^2 + \hat{\alpha}_1/(1 + K_{x,1}x_1)^4}$$

$$- (\phi_1 Y_1 V_{s,1}\sigma_1 e_1 + \phi_2 Y_2 V_{s,2}\sigma_2 e_2)e_1, \tag{18}$$

$$\frac{dg}{dt} = V_{e,1} \frac{1}{1 + \alpha_1/(1 + K_{x,1}x_1)^2 + \hat{\alpha}_1/(1 + K_{x,1}x_1)^4}$$

$$- (\phi_1 Y_1 V_{s,1}\sigma_1 e_1 + \phi_2 Y_2 V_{s,2}\sigma_2 e_2)g, \tag{19}$$

$$\frac{de_2}{dt} = V_{e,2} \frac{1}{1 + \alpha_2/(1 + K_{x,2}x_2)} - (\phi_1 Y_1 V_{s,1}\sigma_1 e_1 + \phi_2 Y_2 V_{s,2}\sigma_2 e_2)e_2, \tag{20}$$

$$x_i = \frac{V_{s,i}}{k_{x,i}^+ + k_{x,i}^-} e_i \sigma_i, \tag{21}$$

where

$$\sigma_i \equiv \frac{s_{i,0}}{K_{s,i} + s_{i,0}}, \qquad \phi_i \equiv \frac{k_{x,i}^+}{k_{x,i}^- + k_{x,i}^+}.$$

The parameter, ϕ_i, is the fraction of substrate intake that is channeled into growth and respiration (the remainder is expelled into the medium). The second term in Eqs. (18)–(20) represents the dilution rate of E_1, G, and E_2, respectively.[1]

It follows from (18)–(20) that during single-substrate growth on S_i, the steady state activity of E_i is at most

$$\sqrt{\frac{V_{e,i}}{\phi_i Y_i V_{s,i}\sigma_i}},$$

and the maximum specific growth rate is at most

$$\phi_i Y_i V_{s,i} \sqrt{\frac{V_{e,i}}{\phi_i Y_i V_{s,i}\sigma_i}} \sigma_i = \sqrt{\phi_i Y_i V_{s,i} V_{e,i}\sigma_i}.$$

---

[1]These equations are formally similar to the model considered in Narang and Pilyugin (2007), the main difference being that the induction kinetics were assumed to follow Yagil and Yagil kinetics.

Thus, we are led to define the dimensionless variables

$$\epsilon_i \equiv \frac{e_i}{\sqrt{V_{e,i}/(\phi_i Y_i V_{s,i} \sigma_i)}}, \qquad \gamma \equiv \frac{g}{\sqrt{V_{e,1}/(\phi_1 Y_1 V_{s,1} \sigma_1)}},$$

$$\chi_i \equiv K_{x,i} x_i, \qquad \tau \equiv t\sqrt{\phi_1 Y_1 V_{s,1} V_{e,1} \sigma_1},$$

which yield the dimensionless equations

$$\frac{d\epsilon_1}{d\tau} = \frac{1}{1 + \alpha_1/(1 + \chi_1)^2 + \hat{\alpha}_1/(1 + \chi_1)^4} - (\epsilon_1 + \alpha\epsilon_2)\epsilon_1, \tag{22}$$

$$\frac{d\gamma}{d\tau} = \frac{1}{1 + \alpha_1/(1 + \chi_1)^2 + \hat{\alpha}_G/(1 + \chi_1)^4} - (\epsilon_1 + \alpha\epsilon_2)\gamma, \tag{23}$$

$$\frac{d\epsilon_2}{d\tau} = \alpha \frac{1}{1 + \alpha_2/(1 + \chi_2)} - (\epsilon_1 + \alpha\epsilon_2)\epsilon_2, \tag{24}$$

$$\chi_i = \delta_i \epsilon_i, \quad i = 1, 2 \tag{25}$$

with dimensionless parameters

$$\alpha \equiv \frac{\sqrt{\phi_2 Y_2 V_{s,2} V_{e,2} \sigma_2}}{\sqrt{\phi_1 Y_1 V_{s,1} V_{e,1} \sigma_1}}, \tag{26}$$

$$\delta_i \equiv \delta_{i,m} \sqrt{\sigma_i}, \qquad \delta_{i,m} \equiv \frac{K_{x,i}}{k_{x,i}^- + k_{x,i}^+} \sqrt{\frac{V_{s,i} V_{e,i}}{\phi_i Y_i}}. \tag{27}$$

Here, α, is a measure of the specific growth rate on S_2 relative to that on S_1, and $\delta_{i,m}$ is a measure of the quasi-steady state concentration of X_i at saturating concentrations of S_i (or equivalently, the strength of the positive feedback generated by induction of E_i).

Unlike TMG, lactose is rapidly metabolized to support growth and respiration. It follows that the ability of the cells to accumulate the intracellular substrate, (and hence, the strength of the positive feedback) is smaller during growth on lactose, i.e., $\delta_{1,m} < \bar{\delta}_{1,m}$. Indeed, (11) and (27) imply that

$$\frac{\delta_{1,m}}{\bar{\delta}_{1,m}} = \frac{r_g}{\sqrt{\phi_1 Y_1 V_{s,1} V_{e,1}}} \frac{k_{x,1}^-}{k_{x,1}^- + k_{x,1}^+}.$$

Since r_g, the specific growth rate in the experiments with TMG, is comparable to $\sqrt{\phi_1 Y_1 V_{s,1} V_{e,1}}$, a measure of the maximum specific growth rate on lactose, we have

$$\frac{\delta_{1,m}}{\bar{\delta}_{1,m}} \approx \frac{k_{x,1}^-}{k_{x,1}^- + k_{x,1}^+},$$

which is less than 1.

In the particular case of growth on lactose, $\sigma_2 = \alpha = 0$, and the above equations become

$$\frac{d\epsilon_1}{d\tau} = \frac{1}{1 + \alpha_1/(1 + \chi_1)^2 + \hat{\alpha}_1/(1 + \chi_1)^4} - \epsilon_1^2, \tag{28}$$

$$\frac{d\gamma}{d\tau} = \frac{1}{1 + \alpha_1/(1+\chi_1)^2 + \hat{\alpha}_G/(1+\chi_1^4)} - \epsilon_1\gamma, \tag{29}$$

$$\chi_1 = \delta_1\epsilon_1. \tag{30}$$

Note that (28) is formally similar to (8), the only difference being that the dilution rate is proportional to ϵ_1^2 rather than ϵ_1. This reflects the fact that during growth on lactose, the specific growth rate is proportional to the activity of E_1.

3. Results and discussion

We note at the outset that the steady state GFP level is completely determined by the steady state activity of the *lac* enzymes. More precisely, Eqs. (8), (9) and (22), (23) imply that

$$\frac{\gamma}{\epsilon_1} = \frac{1 + \alpha_1/(1+\chi_1)^2 + \hat{\alpha}_1/(1+\chi_1)^4}{1 + \alpha_1/(1+\chi_1)^2 + \hat{\alpha}_G/(1+\chi_1)^4}, \tag{31}$$

where χ_1 is given by (10) or (25). In what follows, we shall focus on the variation of the steady state enzyme activity, ϵ_1, with the extracellular TMG ($\bar{\delta}_1$) or lactose (δ_1) concentration. Given this relation, the steady state GFP level is completely determined by (31).

If the repression characteristics of the *lac* reporter were identical to those of native *lac* ($\alpha_1 = \alpha_G$, $\hat{\alpha}_1 = \hat{\alpha}_G$), γ would be identical to ϵ_1. However, since $\hat{\alpha}_G = 150$ is significantly smaller than $\hat{\alpha}_1 = 1250$, the ratio, γ/ϵ_1, is a decreasing function of χ_1. Now the inducer levels, χ_1, are vanishingly small in noninduced cells, and very large in induced cells. Hence, (31) implies that

$$\frac{\gamma_{\text{non-induced}}}{\epsilon_{1,\text{non-induced}}} \approx 8, \qquad \frac{\gamma_{\text{induced}}}{\epsilon_{1,\text{induced}}} \approx 1 \quad \Rightarrow \quad \frac{(\gamma_{\text{induced}}/\gamma_{\text{non-induced}})}{(\epsilon_{1,\text{induced}}/\epsilon_{1,\text{non-induced}})} \approx \frac{1}{8},$$

i.e., ratio of the GFP levels in induced and noninduced cells is significantly smaller than the corresponding ratio of the enzyme activities. We shall appeal to this fact later.

In what follows, we consider the growth on TMG, lactose, and lactose + glucose. In the first two cases, we also study the dynamics in the absence of DNA looping ($\hat{\alpha}_1 = 0$). We consider this biologically unrealistic scenario because it yields useful intuitive insights.

### 3.1. Growth on TMG and nongalactosidic carbon sources

3.1.1. No DNA looping
In this case, the enzyme dynamics are given by (8)–(10) with $\hat{\alpha}_1 = 0$, and the steady states satisfy the equation

$$f(\epsilon_1) \equiv \frac{1}{1 + \alpha_1/(1+\bar{\delta}_1\epsilon_1)^2} - \epsilon_1 = 0. \tag{32}$$

Since the induction rate lies between $1/(1+\alpha_1)$ and 1, so does the steady state enzyme activity.

Equation (32) captures the steady state data shown in Fig. 2. Indeed, (32) implies that

$$\bar{\delta}_1(\epsilon_1) \equiv \sqrt{\frac{\alpha_1}{\epsilon_1(1-\epsilon_1)}} - \frac{1}{\epsilon_1}.$$
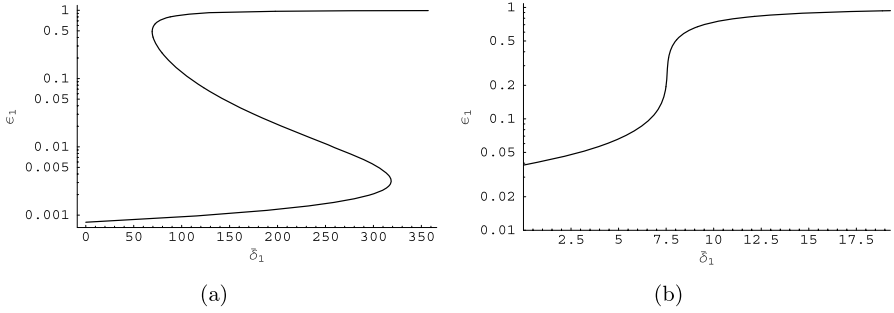
Fig. 6 Variation of the steady state enzyme activity (ϵ_1) with extracellular TMG level ($\bar{\delta}_1$) at high and low repression levels. (a) At high repression levels ($\alpha_1 = 1,200$), there is a range of extracellular TMG concentrations at which the enzyme activity is bistable. (b) At low repression levels ($\alpha_1 = 25$), there is a unique enzyme activity at every extracellular TMG level.

Given any α_1, the parametric curve, $(\bar{\delta}_1(\epsilon_1), \epsilon_1)$, $1/(1 + \alpha_1) < \epsilon_1 < 1$, yields the variation of the steady state enzyme activity with $\bar{\delta}_1$, a surrogate for the extracellular TMG concentration. If the repression is large, the locus of steady states is hysteretic (Fig. 6a). If the repression is small, there is a unique enzyme activity at every extracellular TMG level (Fig. 6b).

The loss of bistability at low repression levels becomes more transparent if we plot the surface of steady states as a function of the parameters, $\alpha_1, \bar{\delta}_1$ (Fig. 7a). The steady states in Fig. 6 were obtained by varying $\bar{\delta}_1$ at fixed α_1. These steady states are represented in Fig. 7a by the intersection of the plane, $\alpha_1 = $ constant, with the surface of steady states. Now at high repression levels, the surface contains two folds (red and blue curves). Thus, the steady states of high-repression cells correspond to a curve with two folds. As the repression level decreases, the two folds approach each other until they merge and disappear. The steady states of low-repression cells, therefore, increase monotonically.

Ozbudak et al. observed that the transition from bistability to monostability occurs at a repression level lying between 5 and 50. We show below that the model captures this result. To this end, we begin by deriving the equations describing the folds of the steady state surface. Evidently, the folds satisfy (32) because they lie on the steady state surface. Since the folds are singular points of the surface, they also satisfy the equation

$$f_{\epsilon_1}(\epsilon_1) = \frac{2\alpha_1 \bar{\delta}_1/(1 + \bar{\delta}_1\epsilon_1)^3}{[1 + \alpha_1/(1 + \bar{\delta}_1\epsilon_1)^2]^2} - 1 = 0. \tag{33}$$

It is shown in Appendix B that Eqs. (32), (33) define a curve in the $\alpha_1\bar{\delta}_1\epsilon_1$-space with the parametric representation

$$\epsilon_1(\chi_1) = \frac{\chi_1 - 1}{2\chi_1}, \qquad \alpha_1(\chi_1) = \frac{(1 + \chi_1)^3}{\chi_1 - 1}, \qquad \bar{\delta}_1(\chi_1) = \frac{2\chi_1^2}{\chi_1 - 1}. \tag{34}$$

As χ_1 increases from 1^+ to ∞, this parametric representation traces the folds of the steady state surface.

The bifurcation diagram for a system refers to the classification of its dynamics in parameter space. For the system at hand, it is obtained by projecting the folds onto the
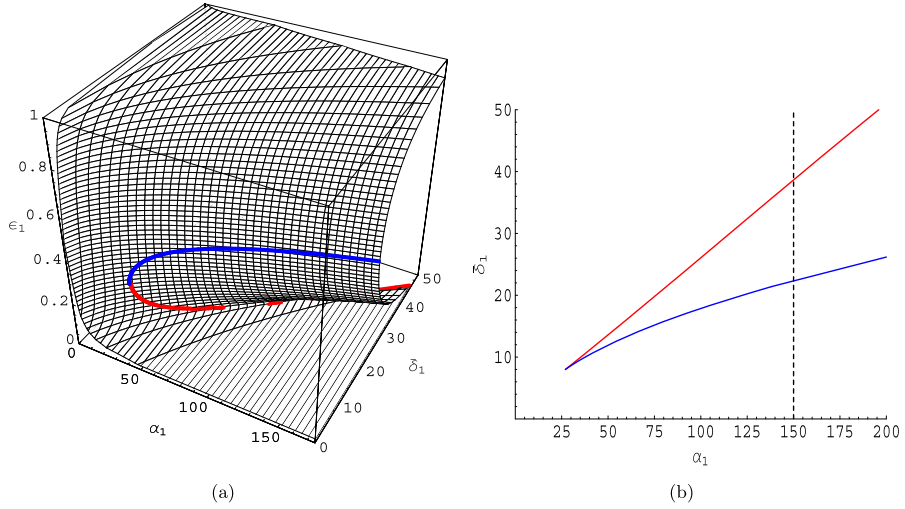
Fig. 7 (a) The surface of steady state enzyme levels for growth on TMG. The surface contains two folds, which are represented by the red and blue curves. (b) The bifurcation diagram for growth on TMG, obtained by projecting the folds in (a) onto the $\alpha_1 \bar{\delta}_1$-plane. Bistability occurs precisely if α_1 and $\bar{\delta}_1$ lie in the region between the red and blue curves. The dashed line show the path along which $\bar{\delta}_1$ changes when a given cell type (fixed α_1) is exposed to various extracellular TMG concentrations. (Color figure online.)

$\alpha_1 \bar{\delta}_1$-plane (Fig. 7b). Evidently, multiple steady states occur precisely when the parameters, α_1 and $\bar{\delta}_1$, lie between the blue and red curves in Fig. 7b. These two curves meet at a cusp characterized by the conditions

$$\frac{d\alpha_1}{d\chi_1} = 2\frac{(1+\chi_1)^2(\chi_1 - 2)}{(\chi_1 - 1)^2} = 0,$$

$$\frac{d\bar{\delta}_1}{d\chi_1} = 2\frac{\chi_1(\chi_1 - 2)}{(\chi_1 - 1)^2} = 0,$$

which imply that the cusp occurs at $\chi_1 = 2$, and its coordinates are $\alpha_1 = 27$, $\bar{\delta}_1 = 8$. It follows that bistability is feasible only if $\alpha_1 > 27$, which lies half-way between the experimentally measured bounds (5 and 50). Thus, the model yields results that are consistent with the data.

Figure 7b is characterized by two properties: (a) There is no bistability at small α_1, and (b) bistability is feasible at high α_1, provided $\bar{\delta}_1$ lies within a finite interval. To a first degree of approximation, these properties reflect the following physical fact: Bistability occurs precisely when the induction rate is cooperative. To see this, observe that to a first degree of approximation, we can identify the existence of cooperative kinetics with the existence of an inflection point on the induction curve. Since the induction rate has an inflection point at $\epsilon_1 = (\sqrt{\alpha_1/3} - 1)/\bar{\delta}_1$, it follows that:

1. If α_1 is small, there is no inflection point. Hence, the induction rate is not cooperative, i.e., its slope decreases monotonically with ϵ_1, and bistability is impossible.

2. If α_1 is large, the induction rate contains an inflection point, but it is cooperative, in effect, only within a finite interval of $\bar\delta_1$. At large $\bar\delta_1$, the inflection point is so close to 0 that the induction rate is not cooperative, except at vanishingly small enzyme levels. At small $\bar\delta_1$, the inflection point is so large compared to 1 that the induction rate is effectively linear on the interval, $0 < \epsilon_1 < 1$, containing the steady state. Thus, bistability is feasible only in a finite interval of $\bar\delta_1$.

In other words, the cooperativity of the quasi-steady state induction rate depends on the intracellular parameter, α_1, and the state of the environment ($\bar\delta_1$ is proportional to σ_1). If α_1 is small, bistability is impossible because there is no extracellular TMG level that can make the induction rate cooperative. If α_1 is large, there is a finite range of extracellular TMG levels at which the induction rate is cooperative, and bistability is feasible.

3.1.2. DNA looping

We assumed above that the repression was entirely due to repressor-operator binding. In reality, the repression is dominated by DNA looping. Since the induction kinetics are qualitatively different in the presence of DNA looping, it is relevant to ask if the foregoing conclusions are dramatically altered when $\hat\alpha_1 > 0$. We show below that the bifurcation diagram is essentially unchanged if $0 < \hat\alpha_1 < 16$, but it is qualitatively different for larger values of $\hat\alpha_1$.

In the presence of DNA looping, the steady states are given by the equation

$$\frac{d\epsilon_1}{d\tau} = f(\epsilon) \equiv \frac{1}{1 + \alpha_1/(1 + \bar\delta_1\epsilon_1)^2 + \hat\alpha_1/(1 + \bar\delta_1\epsilon_1)^4} - \epsilon_1 = 0.$$

For each fixed $\hat\alpha_1 \geq 0$, this equation defines the steady state surface in the $\alpha_1\bar\delta_1\epsilon_1$-space. The folds on the steady state surface also satisfy the equation

$$f_{\epsilon_1}(\epsilon_1) = \frac{2\alpha_1\bar\delta_1/(1 + \bar\delta_1\epsilon_1)^3 + 4\hat\alpha_1\bar\delta_1/(1 + \bar\delta_1\epsilon_1)^5}{[1 + \alpha_1/(1 + \bar\delta_1\epsilon_1)^2 + \hat\alpha_1/(1 + \bar\delta_1\epsilon_1)^4]^2} - 1 = 0.$$

It is shown in Appendix B that the folds have the parametric representation

$$\alpha_1(\chi_1) = \frac{1}{(1 + \chi_1)^2} \frac{\hat\alpha_1(3\chi_1 - 1) - (1 + \chi_1)^5}{(1 - \chi_1 t)},$$

$$\epsilon_1(\chi_1) = \frac{1}{2\chi_1} \frac{1 - \chi_1}{\hat\alpha_1/(1 + \chi_1)^4 - 1},$$

$$\bar\delta_1(\chi_1) = \frac{\chi_1}{\epsilon_1(\chi_1)} = 2\chi_1^2 \frac{\hat\alpha_1/(1 + \chi_1)^4 - 1}{1 - \chi_1}.$$

Furthermore, bistability is feasible at every $\hat\alpha_1 \geq 0$, but there are three types of bifurcation diagrams:

1. If the repression due to DNA looping is small ($\hat\alpha_1 < (5/3)^5 \approx 12.8$), the bifurcation diagram is similar to the one obtained in the absence of DNA looping: Bistability is feasible only if α_1 is sufficiently large; moreover, even if this condition is satisfied, bistability occurs within a finite interval of $\bar\delta_1$ (Fig. B.1a).
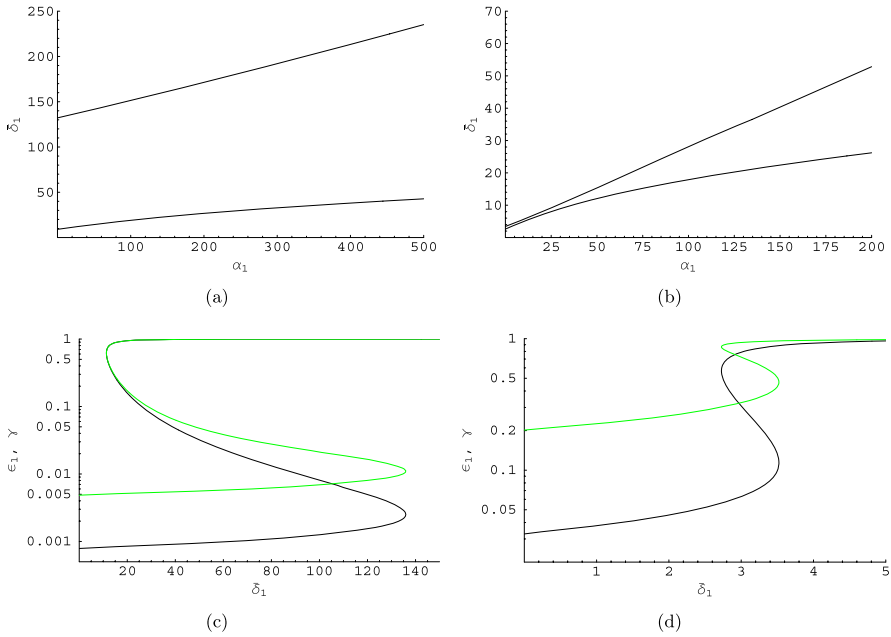
Fig. 8 *Upper panel:* Bifurcation diagrams for growth on TMG of (a) wild-type cells ($\hat{\alpha}_1 = 1, 250$), and (b) low-repression cells ($\hat{\alpha}_1 = 30$). *Lower panel:* Variation of the steady state enzyme activity (black curve) and fluorescence intensity (green curve) with the extracellular TMG concentration ($\bar{\delta}_1$) for (c) wild-type cells ($\hat{\alpha}_1 = 1, 250$, $\alpha_1 = 20$), and (d) low-repression cells ($\hat{\alpha}_1 = 30$, $\alpha_1 = 0$). (Color figure online.)

2. At intermediate levels of repression ($(5/3)^5 < \hat{\alpha}_1 < 16$), the bifurcation diagram contains two distinct bistable regions (Fig. B.1b). However, one of these regions is so small that it is unlikely to be observed in practice.

3. If the repression due to DNA looping is large ($\hat{\alpha}_1 > 16$), the bifurcation diagram is qualitatively different: Bistability is feasible at every $\alpha_1 \geq 0$ (Figs. 8a, b). This reflects the fact that if the repression due to DNA looping is sufficiently large, the induction rate is cooperative even if there is no repression due to repressor-operator binding.

Thus, for all practical purposes, there are only two types of bifurcation diagrams.

The simulations are consistent with the data shown in Fig. 2a. In wild-type cells, bistability occurs over the range $10 \lesssim \bar{\delta}_1 \lesssim 130$ (Fig. 8c), which is in reasonable agreement with the 10-fold range observed in the experiments (3–30 μM in Fig. 2a).

At parameter values corresponding to the cells transfected with the *lac* operator ($\alpha_1 \approx 0$, $\hat{\alpha}_1 \approx 30$), there is bistability, but the range of extracellular concentrations supporting bistability is so small that the system is practically monostable (Fig. 8d). However, the model cannot be compared to the data shown in Fig. 2b, since it does not account for the diffusive flux of TMG, which is significant at extracellular TMG concentrations exceeding 50 μM.

We can estimate $\bar{\delta}_{1,m}$ by comparing the model prediction with the experimental data. Figures 8c and 2a show that at the upper fold point, $\bar{\delta}_1 \approx 130$, and $s_{1,0} \approx 30$ μM, respectively. Since $K_{s,1} = 680$ μM (Ozbudak et al., 2004)

$$130 \approx \bar{\delta}_1 = \bar{\delta}_{1,m} \frac{30}{680 + 30} \quad \Rightarrow \quad \bar{\delta}_{1,m} \sim 3100.$$

This estimate is consistent with the experimental data. Indeed, the model implies that at saturating concentrations of extracellular TMG, the intracellular concentration of TMG is $K_x^{-1}\bar{\delta}_{1,m}$. Since $K_x^{-1} \sim 7$ μM (Oehler et al., 2006, Fig. 4B), the intracellular TMG concentration at saturating conditions is 20 mM, which is in reasonable agreement with the experimentally measured value of 15 mM (Kepes, 1960, Fig. 5).

3.2. Growth on lactose

3.2.1. No DNA looping
In the presence of lactose, the steady states satisfy the equation

$$g(\epsilon_1) \equiv \frac{1}{1 + \alpha_1/(1 + \delta_1\epsilon_1)^2} - \epsilon_1^2 = 0, \tag{35}$$

which defines the steady state surface in the $\alpha_1\delta_1\epsilon_1$-space.

It is clear that no matter what the parameter values, there is at least one steady state. Indeed, (35) implies that the net rate of enzyme synthesis, $g(\epsilon_1)$, is positive if $\epsilon_1 = 0$, and negative if ϵ_1 is sufficiently large. It follows that there is at least one $1/(1 + \alpha_1) < \epsilon_1 < 1$ at which $g(\epsilon_1)$ is zero.

It turns out, however, there is exactly one steady state because multiple steady states are impossible. To see this, observe that multiple steady states are feasible only if the steady state surface contains singular points, i.e., there are points $\alpha_1, \delta_1, \epsilon_1 > 0$ satisfying (35) and the necessary condition

$$g_{\epsilon_1}(\epsilon_1) = \frac{1}{[1 + \alpha_1/(1 + \delta_1\epsilon_1)^2]^2} \frac{2\alpha_1\delta_1}{(1 + \delta_1\epsilon_1)^3} - 2\epsilon_1 = 0. \tag{36}$$

But there are no such points because $g_{\epsilon_1} < 0$ at every point on the steady state surface. Indeed, (35) implies that every point on the steady state surface satisfies the relations

$$\frac{1}{[1 + \alpha_1(1 + \delta_1\epsilon_1)^2]^2} = \epsilon_1^4, \qquad \frac{\alpha_1}{(1 + \delta_1\epsilon_1)^2} = \frac{1}{\epsilon_1^2} - 1.$$

Substituting these relations in (36) yields

$$g_{\epsilon_1}(\epsilon_1) = 2\epsilon_1\left[(1 - \epsilon_1^2)\frac{\delta_1\epsilon_1}{1 + \delta_1\epsilon_1} - 1\right] < 0. \tag{37}$$

It follows that there are no singular points on the steady state manifold, and hence, no multiple steady states.

We pause for a moment to give the physical meaning of the foregoing mathematical argument. To this end, observe that bistability can occur only if the system permits the
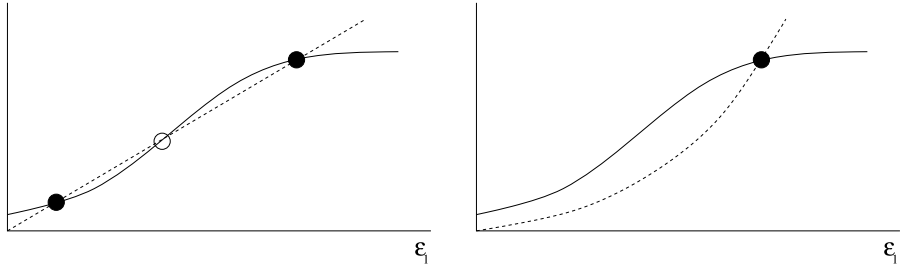
Fig. 9 Intuitive explanation for the absence of bistability during growth on lactose of cells lacking DNA looping. The enzyme synthesis and dilution rates are represented by full and dashed lines, respectively. Stable and unstable steady states are represented by full and open circles, respectively. (a) During growth on TMG, bistability is feasible because the dilution rate is proportional to the enzyme level. (b) During growth on lactose, bistability is infeasible because the stabilizing effect of dilution (ϵ_1^2) is so strong that an unstable steady state (and hence, bistability) is infeasible.

existence of an unstable steady state, i.e., a steady state at which the slope of the induction rate exceeds the slope of the dilution rate (Fig. 9a).[2] Such a steady state is feasible when the cells are grown in the presence of TMG because the dilution rate increases linearly with the enzyme level. It is infeasible during growth on lactose because the dilution rate, ϵ_1^2, increases so rapidly with the enzyme level that at every conceivable steady state, the slope of the dilution rate exceeds the slope of the induction rate, i.e., $g_{\epsilon_1} < 0$ at every possible steady state (Fig. 9b). In other words, the stabilizing effect of dilution is so strong that an unstable stable steady state, and hence, bistability, is impossible.

The model assumes that the yield is constant. It is well known, however, that the yield is vanishingly small under starvation conditions, and increases progressively as the nutritional status of the cells improves (Tempest et al., 1967). Thus, it seems plausible to assume that at low enzyme levels, the lactose transport rate and yield are relatively small; as the enzyme level increases, so do the lactose transport rate and the yield. If this is true, it is relevant to ask if multistability is impossible even if the yield is an increasing function of the enzyme level, i.e., the yield has the form $Y_1\phi(\epsilon_1)$, where $\phi(\epsilon_1) \leq 1$ is some increasing function of ϵ_1. The foregoing physical explanation suggests that multistability is, a fortiori, impossible because the dilution rate now increases with ϵ_1 at a rate even faster than ϵ_1^2. Analysis confirms this intuitive argument—the value of g_{ϵ_1} at any point on the steady state surface is

$$2\phi(\epsilon_1)\epsilon_1\left[\left\{1 - \phi(\epsilon_1)\epsilon_1^2\right\}\frac{\delta_1\epsilon_1}{1+\delta_1\epsilon_1} - 1\right] - \phi_{\epsilon_1}(\epsilon_1)\epsilon_1^2 < 0.$$

Thus, multistability is impossible even if the yield is an increasing function of the enzyme level.

---

[2]The stability of a steady state is completely determined by the relative slopes of the induction and dilution rates at the steady state. If the slope of the induction rate at a steady state exceeds the corresponding slope of the dilution rate (see open circle in Fig. 9a), the slightest increase (resp., decrease) in the enzyme level increases (resp., decreases) the induction rate more than the dilution rate, so that the enzyme level grows (resp., declines) even further.

The above argument shows that the existence of bistability is not determined solely by the intensity of the destabilizing positive feedback generated by induction. It also depends on the strength the stabilizing effect of dilution. If this stabilizing effect is sufficiently large, it can neutralize the destabilizing effect of positive feedback.

3.2.2. DNA looping

We have shown above that in the absence of DNA looping, there is no bistability during growth on lactose because the dilution rate, which is proportional to ϵ_1^2, neutralizes the destabilizing effect of positive feedback. However, in the presence of DNA looping, the destabilizing effect of positive feedback is much stronger because the induction rate contains terms proportional to ϵ_1^4. Under these conditions, it seems plausible to expect that bistability is feasible at sufficiently large $\hat{\alpha}_1$. We show below that is indeed the case, but the bistable region is extremely small.

In the presence of DNA looping, the bifurcation points satisfy the equations

$$g(\epsilon_1) \equiv \frac{1}{1 + \alpha_1/(1 + \delta_1\epsilon_1)^2 + \hat{\alpha}_1/(1 + \delta_1\epsilon_1)^4} - \epsilon_1^2 = 0,$$

$$g_{\epsilon_1}(\epsilon_1) = \frac{2\alpha_1\delta_1/(1 + \delta_1\epsilon_1)^3 + 4\hat{\alpha}_1\delta_1/(1 + \delta_1\epsilon_1)^5}{[1 + \alpha_1/(1 + \delta_1\epsilon_1)^2 + \hat{\alpha}_1/(1 + \delta_1\epsilon_1)^4]^2} - 2\epsilon_1 = 0.$$

For each fixed $\hat{\alpha}_1 > 0$, these two equations define the locus of the bifurcation points in $\alpha_1\delta_1\epsilon_1$-space. It is shown in Appendix C that this curve has the parametric representation

$$\epsilon_1(\chi_1) = \sqrt{\frac{1}{\chi_1\{\hat{\alpha}_1/(1 + \chi_1)^4 - 1\}}},$$

$$\alpha_1(\chi_1) = \frac{\hat{\alpha}_1(\chi_1 - 1) - (1 + \chi_1)^5}{(1 + \chi_1)^2},$$

$$\delta_1(\chi_1) = \frac{\chi_1}{\epsilon_1(\chi_1)} = \chi_1^{3/2}\sqrt{\frac{\hat{\alpha}_1}{(1 + \chi_1)^4} - 1}.$$

Furthermore, bistability is feasible only if $\hat{\alpha}_1 > 5^5/2^4 \approx 195$.

In wild-type cells, for instance, bistability occurs for all $7 \lesssim \delta_1 \lesssim 9$ (Fig. 10a). Now it is conceivable that bistability is not observed during growth on lactose because the strength of the positive feedback, $\delta_{1,m}$, is so small (<7) that $\delta_1 \equiv \delta_{1,m}\sigma_1$ remains below the bistable region at all concentrations of extracellular lactose. It is clear, however, that even if $\delta_{1,m}$ is large (>9), the bistable region is so narrow that it is unlikely to be observed in practice (Fig. 10b). We show below that the width of the bistable region increases dramatically in the presence of glucose.

In wild-type cells, bistability is feasible during growth on lactose, but the bifurcation diagram is qualitatively different from that obtained during growth on TMG. Indeed, during growth on TMG, bistability is feasible for all $\alpha_1 \geq 0$ (Fig. 8a). In sharp contrast, bistability is feasible during growth on lactose only if α_1 is sufficiently small (Fig. 10a). The qualitatively different bifurcation diagram for lactose can be explained as follows.
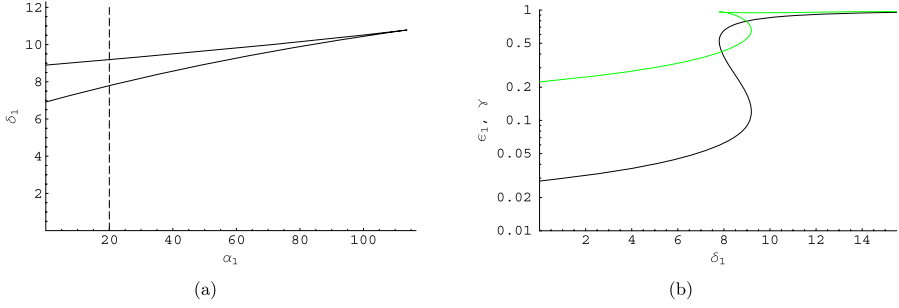
Fig. 10 Growth of wild-type cells on lactose: (a) Bifurcation diagram ($\hat{\alpha}_1 = 1,250$). The dashed line shows the path along which δ_1 changes when the extracellular lactose concentration is varied. (b) The variation of the steady state enzyme activity (black curve) and fluorescence intensity (green curve) with δ_1, a surrogate for the extracellular lactose concentration ($\hat{\alpha}_1 = 1,250$, $\alpha_1 = 20$). (Color figure online.)

During growth on lactose, bistability can occur only if DNA looping has a strong effect on the induction rate. But DNA looping dominates the induction rate precisely if

$$\frac{\hat{\alpha}_1}{(1 + \chi_1)^4} \gg \frac{\alpha_1}{(1 + \chi_1)^2} \quad \Rightarrow \quad \chi_1 \ll \sqrt{\frac{\hat{\alpha}_1}{\alpha_1}} - 1.$$

It follows that regardless of the value of $\hat{\alpha}_1$, the range of inducer concentrations at which DNA looping is dominant vanishes at a sufficiently high value of α_1. Consequently, the induction rate, and hence, the dynamics, become similar to those observed in the absence of DNA looping.

3.3. Growth on lactose + glucose

In the presence of glucose and lactose, the steady states satisfy the equations

$$g_1(\epsilon_1, \epsilon_2) \equiv \frac{1}{1 + \alpha_1/(1 + \delta_1\epsilon_1)^2 + \hat{\alpha}_1/(1 + \delta_1\epsilon_1)^4} - (\epsilon_1 + \alpha\epsilon_2)\epsilon_1 = 0, \qquad (38)$$

$$g_2(\epsilon_1, \epsilon_2) \equiv \frac{\alpha}{1 + \alpha_2/(1 + \delta_2\epsilon_2)} - (\epsilon_1 + \alpha\epsilon_2)\epsilon_2 = 0. \qquad (39)$$

Our goal is to address the following question: Given a particular cell type, what are concentrations of lactose and glucose at which bistability is feasible? This question is difficult to address because there are three parameters that depend on the substrate concentrations ($\delta_i \propto \sqrt{\sigma_i}$, $\alpha \propto \sqrt{\sigma_2/\sigma_1}$). Since the combination of parameters

$$\beta \equiv \frac{\alpha\delta_1}{\delta_2} = \frac{Y_2 k_{x,2}^+ K_{x,2}^{-1}}{Y_1 k_{x,1}^+ K_{x,1}^{-1}}$$

is independent of the substrate concentrations, it is convenient to replace α with $\beta\delta_2/\delta_1$. In terms of the model, the question of interest then becomes: Given any fixed $\alpha_1, \hat{\alpha}_2, \alpha_2, \beta$, what are the values of δ_1 and δ_2 at which bistability is feasible? Unlike $\alpha_1, \hat{\alpha}_2, \alpha_2$, the
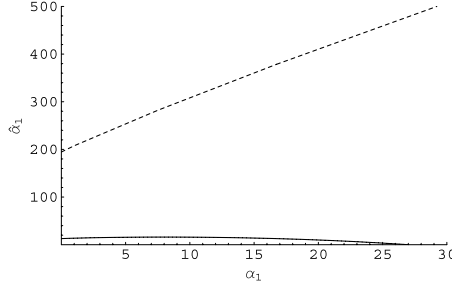
Fig. 11 Classification of the dynamics during growth on lactose + glucose. Bistability is feasible if and only if α_1 and $\hat{\alpha}_1$ lie above the full curve. If α_1 and $\hat{\alpha}_1$ lie between the full and dashed curves (resp., above the dashed curve), the bifurcation diagram has the form shown in Fig. D.1 (resp., Fig. 12a).

value of β cannot be determined from the experimental literature, since $K_{x,2}^{-1}$ is a phenomenological parameter. In the simulations, we assume that $\beta = 1$. However, we show below that this is not a particularly restrictive assumption, since the qualitative behavior of the bifurcation diagram is completely determined by α_1 and $\hat{\alpha}_1$.

Bistability is feasible only if there are steady states satisfying (38), (39) and the condition

$$\det \begin{bmatrix} \frac{\partial g_1}{\partial \epsilon_1} & \frac{\partial g_1}{\partial \epsilon_2} \\ \frac{\partial g_2}{\partial \epsilon_1} & \frac{\partial g_2}{\partial \epsilon_2} \end{bmatrix} = 0.$$

It is shown in Appendix D that these three equations can be rewritten as

$$\delta_1(\chi_1, \chi_2) = \chi_1 \sqrt{1 + \alpha_1/(1 + \chi_1)^2 + \hat{\alpha}_1/(1 + \chi_1)^4} \sqrt{\frac{1}{1 + h(\chi_1, \chi_2)}}, \tag{40}$$

$$\delta_2(\chi_1, \chi_2) = \chi_2 \sqrt{1 + \alpha_2/(1 + \chi_2)} \sqrt{\frac{1 + h(\chi_1, \chi_2)}{h(\chi_1, \chi_2)}}, \tag{41}$$

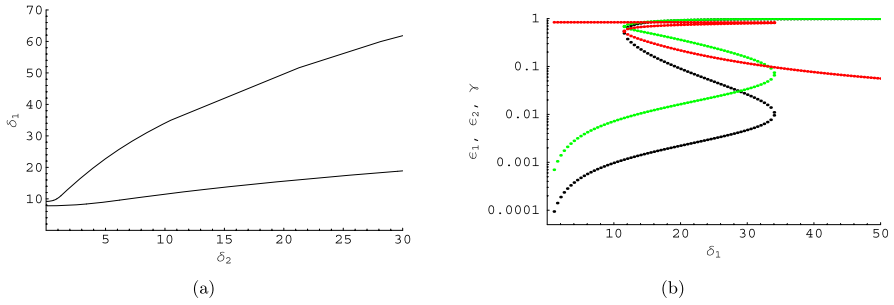$$\beta = \frac{\chi_1}{\chi_2} h(\chi_1, \chi_2), \tag{42}$$

where

$$h(\chi_1, \chi_2) \equiv \frac{1/p(\chi_1) - 1}{1 - q(\chi_2)},$$

$$p(\chi_1) = 2 \frac{\alpha_1/(1 + \chi_1)^2 + 2\hat{\alpha}_1/(1 + \chi_1)^4}{1 + \alpha_1/(1 + \chi_1)^2 + \hat{\alpha}_1/(1 + \chi_1)^4} \frac{\chi_1}{1 + \chi_1} - 1,$$

$$q(\chi_2) = \frac{\alpha_2/(1 + \chi_2)}{1 + \alpha_2/(1 + \chi_2)} \frac{\chi_2}{1 + \chi_2} - 1.$$

Furthermore, bistability is feasible if and only if α_1 and $\hat{\alpha}_1$ lie above the full curve shown in Fig. 11. It is precisely for such values of α_1 and $\hat{\alpha}_1$ that Eq. (42) has positive solutions, which determine a curve in the $\chi_1\chi_2$-space. The variation of $\delta_1(\chi_1, \chi_2)$ and $\delta_2(\chi_1, \chi_2)$

Fig. 12 Steady states of wild-type cells during growth on glucose and lactose ($\alpha_1 = 20$, $\hat{\alpha}_1 = 1,250$, $\alpha_2 = 4$, $\beta = 1$). (a) Bifurcation diagram. Bistability occurs if δ_1, δ_2 lie in the region between the curves. (b) Variation of the steady state activities of E_1 (black curve), E_2 (red curve) and G (green curve) with the extracellular lactose concentration, δ_1, at the fixed glucose concentration, $\delta_2 = 10$. (Color figure online.)

along this curve circumscribes the bistability region on the $\delta_1\delta_2$-plane (for the cell type defined by the fixed values of α_1, $\hat{\alpha}_1$, α_2, β). If α_1 and $\hat{\alpha}_1$ lie between the full and dashed curves of Fig. 11, the bifurcation curve has the form shown in Fig. D.1—it does not intersect the δ_1-axis. If α_1 and $\hat{\alpha}_1$ lie above the dashed curve of Fig. 11, the bifurcation curves intersect the δ_1-axis (Fig. 12a). Thus, the form of the bifurcation curve is completely determined by α_1 and $\hat{\alpha}_1$.

Figure 11 implies that in cells lacking DNA looping, bistability is feasible if and only if $\hat{\alpha}_1$ exceeds the threshold value of 27, which is identical to the threshold in such cells when they grow in the presence of TMG (Fig. 7). The existence of this identity is not coincidental. As we show below, the dynamics of growth on lactose + glucose are, in some sense, identical to the dynamics of growth in the presence of TMG.

Figure 12a shows the bifurcation diagram for wild-type cells growing on lactose + glucose. Evidently, bistability is feasible at every $\delta_2 \geq 0$. This mirrors the fact that during growth of wild-type cells on pure lactose ($\delta_2 = 0$), bistability is feasible, although the range of lactose concentrations supporting bistability is very small. At relatively modest values of the extracellular glucose concentration, δ_2, the bistable region increases dramatically. This is because at sufficiently large concentrations of glucose, the dilution rate due to growth on glucose becomes significant. Importantly, this dilution rate is formally similar to the dilution rate during growth on TMG, insofar as it increases linearly with ϵ_1. Thus, the dynamics are also analogous to those observed during growth on TMG: Bistability is feasible for a range of lactose concentrations (δ_1).

Figure 12a is qualitatively similar to the bifurcation diagram obtained by Santillán et al. (2007, Fig. 2). However, in their model, the width of the bistability region increases in the presence of glucose due to regulatory effects, such as cAMP activation and inducer exclusion, exerted on the induction rate of the *lac* operon. In our model, the same phenomenon occurs because the stabilizing effect of dilution is significantly smaller during growth on lactose + glucose (as opposed to growth on pure lactose).

It remains to explain the discrepancy between the data obtained Ozbudak et al. and Loomis and Magasanik. The simplest explanation is that in the strain used by Ozbudak et al., the parameter, $\delta_{1,m}$, which measures the strength of the positive feedback, is so small (<7) that $\delta_1 \equiv \delta_{1,m}\sigma_1$ does not enter the bistability region at any extracellular lactose

concentration (Fig. 12a). On the other hand, the values of $\delta_{1,m}, \delta_{2,m}$ for the strain used by Loomis and Magasanik are so large that δ_1, δ_2 lie in the bistable region at the extracellular lactose and glucose concentrations used in their experiments.

It should be noted, however, that the discrepancy could also reflect technical differences in the experiments. Figure 12b shows the steady state levels of the lactose enzymes (black curve), glucose enzymes (red curve), and GFP (green curve). In the neighborhood of the upper bifurcation point ($\delta_1 \approx 35$), the lactose enzyme level of the induced cells is ~100 times the lactose enzyme levels of the noninduced cells. However, the GFP level of the induced cells is no more than ~10–20 fold higher than the GFP level of the noninduced cells. Now Fig. 2a shows that in the neighborhood of the upper bifurcation point, the steady state fluorescence of the noninduced cells is scattered over a ~50-fold range (see the fluorescence distribution in lower panel of Fig. 2a over the range 20–30 μM). Assuming that the distribution has a similar variance during growth on lactose, it is conceivable that even if bistability exists, the fluorescence distributions of the noninduced and induced cells overlap, and appear to be unimodal.

In Fig. 12b, the precise values of the *lac* enzyme and GFP levels in induced and noninduced cells depend on the particular choice of the parameter values. However, as shown above, the ratio of GFP levels in induced and noninduced cells is always smaller than the corresponding ratio for the *lac* enzymes. Experimental artefacts indicating the absence of bistability are, therefore, more likely if GFP levels, rather than enzyme activities, are measured.

4. Conclusions

The experimental data shows that the existence of bistability in the *lac* operon depends on the composition of nutrient medium. It occurs during growth on TMG/succinate, but not on lactose. There are conflicting reports of its existence in media containing lactose and glucose.

The occurrence or absence of bistability reflects the net result of the destabilizing effect due to the positive feedback generated by induction and the stabilizing effect of dilution. In previous models, the experimental data has been rationalized entirely in terms of changes in the strength of positive feedback as a function of the medium composition. We have shown above that:

1. The stabilizing effect of dilution also changes dramatically with the composition of the medium. In the presence of nongalactosidic carbon sources, such as succinate or glucose, the dilution rate of the *lac* enzymes contains a term that is proportional to the activity of these enzymes. During growth on pure lactose, the dilution rate of *lac* enzymes is proportional to the square of their activity.
2. These variations in the functional form of the dilution rate have a profound effect on the dynamics. During growth on lactose, the stabilizing effect of dilution is so strong that bistability is virtually impossible even if induction is subject to the strong positive feedback generated by DNA looping. During growth on TMG/succinate or lactose + glucose, bistability is feasible because the stabilizing effect of dilution decreases sharply. Thus, bistabililty is much more likely in the presence of nongalactosidic carbon sources, namely, succinate and glucose.

3. The conflicting results on bistability during growth on lactose + glucose can be explained in terms of the relative magnitudes of the destabilizing and stabilizing effects of positive feedback and dilution, respectively. However, the criterion used by Ozbudak et al. to infer monostability, namely, the absence of a bimodal distribution in noninduced cells, is prone to error. Since the repression of the reporter *lac* operon is much lower than the repression of the native *lac* operon, the ratio of GFP levels in induced and noninduced cells is significantly lower than the corresponding ratio of the enzyme activities. The fluorescence distribution can, therefore, appear to be unimodal even if the enzyme levels are bistable.

Taken together, these results show that while the intensity of the positive feedback undoubtedly influences the dynamics of the *lac* operon, the dilution rate also has profound effects. These effects can be discerned only if it is recognized that the specific growth rate is not a fixed parameter—it depends on the physiological state of the cells.

Acknowledgements

Appendix A: Derivation of Eqs. (18)–(21)

Since $x_1 + x_2 + e_1 + g + e_2 + c^- = 1$, addition of Eqs. (13)–(17) yields

$$0 = r_g - \frac{1}{c}\frac{dc}{dt},$$

where

$$r_g \equiv \sum_{i=1}^{2}\left[V_{s,i}e_i\frac{s_i}{K_{s,i}+s_i} - k_{x,i}^{-}x_i - (1-Y_i)k_{x,i}^{+}x_i\right]$$

is the specific growth rate. This becomes evident if we rewrite the above equation in the more familiar form

$$\frac{dc}{dt} = r_g c.$$

Alternatively, one can see that as expected, r_g is the *net* rate of uptake of the two substrates (uptake minus loss by excretion and respiration).

If the experiments are started with extremely small inocula and terminated before the cell densities become significantly large, the substrate concentrations do not change significantly over the course of the experiment, i.e. $s_i(t) \approx s_{i,0} \equiv s_i(0)$ for all t. Since $k_{x,i}^{+} > k_{x,i}^{-}$ is large, x_i rapidly attains quasisteady state, i.e., Eq. (13) becomes

$$0 \approx V_{s,i}e_i\frac{s_{i,0}}{K_{s,i}+s_{i,0}} - k_{x,i}^{-}x_i - k_{x,i}^{+}x_i,$$

which implies that

$$x_i \approx \frac{V_{s,i}}{k_{x,i}^+ + k_{x,i}^-} e_i \sigma_i, \quad \sigma_i \equiv \frac{s_{i,0}}{K_{s,i} + s_{i,0}}, \tag{A.1}$$

$$r_g \approx \sum_{i=1}^{2} Y_i k_{x,i}^+ x_i = \sum_{j=1}^{2} Y_i \phi_i V_{s,i} e_i \sigma_i, \quad \phi_i \equiv \frac{k_{x,i}^+}{k_{x,i}^- + k_{x,i}^+}. \tag{A.2}$$

Equation (A.1) is identical to Eq. (21). Since $(1/c)(dc/dt) = r_g$, substituting (A.2) in (14)–(16) yields (18)–(20).

Appendix B: Bifurcation diagram for growth in the presence of TMG

The bifurcation points satisfy the equations

$$f(\epsilon_1) \equiv \frac{1}{1 + \alpha_1/(1 + \bar{\delta}_1\epsilon_1)^2 + \hat{\alpha}_1/(1 + \bar{\delta}_1\epsilon_1)^4} - \epsilon_1 = 0,$$

$$f_{\epsilon_1}(\epsilon_1) = \frac{2\alpha_1\bar{\delta}_1/(1 + \bar{\delta}_1\epsilon_1)^3 + 4\hat{\alpha}_1\bar{\delta}_1/(1 + \bar{\delta}_1\epsilon_1)^5}{[1 + \alpha_1/(1 + \bar{\delta}_1\epsilon_1)^2 + \hat{\alpha}_1/(1 + \bar{\delta}_1\epsilon_1)^4]^2} - 1 = 0,$$

which imply that

$$\frac{\alpha_1}{(1 + \bar{\delta}_1\epsilon_1)^2} + \frac{\hat{\alpha}_1}{(1 + \bar{\delta}_1\epsilon_1)^4} = \frac{1}{\epsilon_1} - 1,$$

$$\frac{\alpha_1}{(1 + \bar{\delta}_1\epsilon_1)^2} + 2\frac{\hat{\alpha}_1}{(1 + \bar{\delta}_1\epsilon_1)^4} = \frac{1}{2}\left(1 + \frac{1}{\bar{\delta}_1\epsilon_1}\right)\frac{1}{\epsilon_1}.$$

Since $\chi_1 \equiv \bar{\delta}_1\epsilon_1$, we have two equations that are linear with respect to α_1, $\hat{\alpha}_1$, and $1/\epsilon_1$. Solving for α_1 and $1/\epsilon_1$ in terms of $\hat{\alpha}_1$ and χ_1 yields

$$\alpha_1(\chi_1) = \frac{1}{(1 + \chi_1)^2} \frac{\psi_1(\chi_1)}{1 - \chi_1}, \quad \psi_1(\chi_1) \equiv \hat{\alpha}_1(3\chi_1 - 1) - (1 + \chi_1)^5,$$

$$\epsilon_1(\chi_1) = \frac{1}{2\chi_1} \frac{1 - \chi_1}{\psi_2(\chi_1)}, \quad \psi_2(\chi_1) \equiv \frac{\hat{\alpha}_1}{(1 + \chi_1)^4} - 1,$$
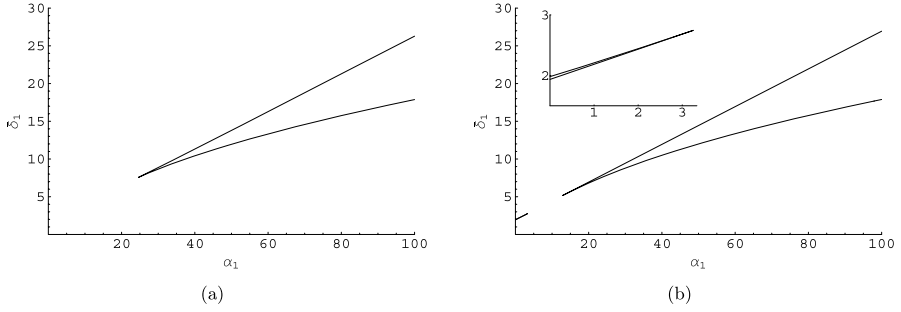
$$\bar{\delta}_1(\chi_1) = \frac{\chi_1}{\epsilon_1(\chi_1)} = 2\chi_1^2 \frac{\psi_2(\chi_1)}{1 - \chi_1}.$$

These three equations provide a parametric representation of the bifurcation curve.

In the absence of DNA looping, the parametric representation of the curve becomes

$$\epsilon_1(\chi_1) = \frac{\chi_1 - 1}{2\chi_1}, \quad \alpha_1(\chi_1) = \frac{(1 + \chi_1)^3}{\chi_1 - 1}, \quad \bar{\delta}_1(\chi_1) = \frac{2\chi_1^2}{\chi_1 - 1}.$$

It follows that the bifurcation curve exists (i.e., lies in the positive octant of the $\alpha_1\bar{\delta}_1\epsilon_1$-space) for all $\chi_1 > 1$.

Fig. B.1 Bifurcation diagrams for growth on TMG in the presence of DNA looping: (a) $\hat{\alpha}_1 = 4$, (b) $\hat{\alpha}_1 = 15$. The inset in (b) shows a blow-up of the bifurcation curve in the region, $\alpha_1 \lesssim 3$.

To determine the existence of bistability in the presence of DNA looping, we begin by observing that $\epsilon_1(\chi_1) > 0$ whenever $\bar{\delta}_1(\chi_1) > 0$. Hence, it suffices to confine our attention to $\alpha_1(\chi_1)$ and $\delta_1(\chi_1)$. But α_1 and δ_1 are positive on the interval $0 < \chi_1 < 1$ (resp., $1 < \chi_1 < \infty$) if and only if ψ_1 and ψ_2 are positive (resp., negative). Thus, we are led to consider the signs of ψ_1 and ψ_2 on $\chi_1 > 0$.

It follows from the analysis of ψ_1 that:

1. If $0 < \hat{\alpha}_1 < (5/3)^5$, then $\psi_1 < 0$ for all $\chi_1 > 0$.
2. If $\hat{\alpha}_1 > (5/3)^5$, then ψ_1 has two positive roots, $0 < \underline{\chi}_1 < \overline{\chi}_1$, and $\psi_1 > 0$ if and only if $\underline{\chi}_1 < \chi_1 < \overline{\chi}_1$. Furthermore, $\underline{\chi}_1, \overline{\chi}_1 < 1$ when $(5/3)^5 < \hat{\alpha}_1 < 16$, and $\underline{\chi}_1 < 1 < \overline{\chi}_1$ when $\hat{\alpha}_1 > 16$.

Similarly, the analysis of ψ_2 shows that:

1. If $0 < \hat{\alpha}_1 < 1$, then $\psi_2 < 0$ for all $\chi_1 > 0$.
2. If $\hat{\alpha}_1 > 1$, then $\psi_2 > 0$ if and only if $0 < \chi_1 < \chi_1^* \equiv \hat{\alpha}_1^{1/4} - 1$. Furthermore, if $\hat{\alpha}_1 > (5/3)^5$, then χ_1^* lies between $\overline{\chi}_1$ and 1.

Taken together, these results imply that there are three distinct types of the bifurcation diagrams:

1. If $0 \leq \hat{\alpha}_1 < (5/3)^5$, then $\alpha_1(\chi_1), \bar{\delta}_1(\chi_1)$ are positive if and only if $\chi_1 > 1$ (Fig. B.1a).
2. If $(5/3)^5 \leq \hat{\alpha}_1 < 16$, then $\bar{\delta}_1(\chi_1), \alpha_1(\chi_1)$ are positive if and only if $\underline{\chi}_1 < \chi_1 < \overline{\chi}_1$ or $\chi > 1$, where $0 < \underline{\chi}_1 < \overline{\chi}_1 < 1$ are the positive roots of $\alpha_1(\chi_1)$. Each of these two intervals of existence yields a bistability region (Fig. B.1b).
3. If $\hat{\alpha}_1 > 16$, then $\bar{\delta}_1(\chi_1), \alpha_1(\chi_1)$ are positive if and only if $\underline{\chi}_1 < \chi < 1$ or $\chi > \overline{\chi}_1$, where $\underline{\chi}_1$ and $\overline{\chi}_1$ are the positive roots of $\alpha_1(\chi_1)$ (Fig. 8a, b).

The geometry of the cusps in the foregoing figures follow from the relations

$$\frac{d\alpha_1}{d\chi_1} = 2\frac{\hat{\alpha}_1(3\chi_1^2 - 3\chi_1 + 2) + (1 + \chi_1)^5(\chi_1 - 2)}{(1 + \chi_1)^3(1 - \chi_1)^2},$$

$$\frac{d\delta_1}{d\chi_1} = \frac{\chi_1}{(1 + \chi_1)^2}\frac{d\alpha_1}{d\chi_1},$$

which imply that there is a cusp whenever $d\alpha_1/d\chi_1 = 0$. It follows from the properties of ψ_1 that there are two cusps if and only if $(5/3)^5 < \hat{\alpha}_1 < 16$. If $\hat{\alpha}_1 > 16$, one of these cusps disappears because its α_1-coordinate is negative.

Appendix C: Bifurcation diagram for growth on lactose

In this case, the bifurcation points satisfy the equations

$$g(\epsilon_1) \equiv \frac{1}{1 + \alpha_1/(1 + \delta_1\epsilon_1)^2 + \hat{\alpha}_1/(1 + \delta_1\epsilon_1)^4} - \epsilon_1^2 = 0,$$

$$g_{\epsilon_1}(\epsilon_1) = \frac{2\alpha_1\delta_1/(1 + \delta_1\epsilon_1)^3 + 4\hat{\alpha}_1\delta_1/(1 + \delta_1\epsilon_1)^5}{[1 + \alpha_1/(1 + \delta_1\epsilon_1)^2 + \hat{\alpha}_1/(1 + \delta_1\epsilon_1)^4]^2} - 2\epsilon_1 = 0,$$

which imply that

$$\frac{\alpha_1}{(1 + \delta_1\epsilon_1)^2} + \frac{\hat{\alpha}_1}{(1 + \delta_1\epsilon_1)^4} = \frac{1}{\epsilon_1^2} - 1,$$

$$\frac{\alpha_1}{(1 + \delta_1\epsilon_1)^2} + 2\frac{\hat{\alpha}_1}{(1 + \delta_1\epsilon_1)^4} = \left(1 + \frac{1}{\delta_1\epsilon_1}\right)\frac{1}{\epsilon_1^2}.$$

Since $\chi_1 = \delta_1\epsilon_1$, we have two equations that are linear with respect to α_1, $\hat{\alpha}_1$, and $1/\epsilon_1^2$. Solving for α_1 and $1/\epsilon_1$ in terms of $\hat{\alpha}_1$ and χ_1 yields

$$\epsilon_1(\chi_1) = \sqrt{\frac{1}{\chi_1\{\hat{\alpha}_1/(1 + \chi_1)^4 - 1\}}},$$

$$\alpha_1(\chi_1) = \frac{\psi_3(\chi_1)}{(1 + \chi_1)^2}, \quad \psi_3(\chi_1) \equiv \hat{\alpha}_1(\chi_1 - 1) - (1 + \chi_1)^5,$$

$$\delta_1(\chi_1) = \frac{\chi_1}{\epsilon(\chi_1)} = \chi_1^{3/2}\sqrt{\frac{\hat{\alpha}_1}{(1 + \chi_1)^4} - 1}.$$

For each fixed $\hat{\alpha}_1 \geq 0$, these relations provide a parametric representation of the bifurcation curve.

In the absence of DNA looping, the bifurcation curve does not exist because the ϵ_1 and δ_1 coordinates of the curve are imaginary (and the α_1-coordinate is negative) for all χ_1.

In the presence of DNA looping, the bifurcation curve exists for all $\hat{\alpha}_1 > 5^5/2^4 \approx 195$. To see this, observe that since

$$\alpha_1(\chi_1) > 0 \quad \Rightarrow \quad \hat{\alpha}_1(\chi_1 + 1) > \hat{\alpha}_1(\chi_1 - 1) > (1 + \chi_1)^5, \tag{C.1}$$

ϵ_1 and δ_1 are positive whenever α_1 is positive. Hence, it suffices to confine our attention to α_1. Now, $\alpha_1 > 0$ if and only $\psi_3 > 0$. One can solve the equations $\psi_3 = d\psi_3/d\chi_1 = 0$ to conclude that $\psi_3 > 0$ for some $\chi_1 > 0$ if and only if $\hat{\alpha}_1 > 5^5/2^4$. In this case, ψ_3 and α_1 have two roots, $0 < \underline{\chi}_1 < \overline{\chi}_1$, and are positive if and only if χ_1 lies between these roots.

The bifurcation diagram is qualitatively similar to Fig. 10a for all $\hat{\alpha}_1 > 5^5/2^4$ because under this condition, α_1 and δ_1 are positive on $(\underline{\chi}_1, \overline{\chi}_1)$, and achieve a unique maximum on $(\underline{\chi}_1, \overline{\chi}_1)$ at the very same value of χ_1. To see this, observe that α_1 has at least one maximum in $(\underline{\chi}_1, \overline{\chi}_1)$. In fact, it has exactly one maximum because

$$\frac{d\alpha_1}{d\chi_1} = \frac{\hat{\alpha}_1(3 - \chi_1) - 3(1 + \chi_1)^5}{(1 + \chi_1)^3}$$

cannot have more than one zero on this interval. On the other hand, $\delta_1 > 0$ on $[\underline{\chi}_1, \overline{\chi}_1]$ because $\delta_1 > \alpha_1$. Furthermore, δ_1 and α_1 attain a maximum at the very same χ_1 because

$$\frac{d\delta_1}{d\chi_1} = \frac{1}{2}\left(\frac{\chi_1}{1 + \chi_1}\right)^2 \frac{1}{\delta_1}\frac{d\alpha_1}{d\chi_1},$$

$$\frac{d^2\delta_1}{d\chi_1^2} = \frac{1}{2\delta_1}\frac{d^2\alpha_1}{d\chi_1^2}.$$

The first relation implies that $d\delta_1/d\chi_1 = 0$ precisely when $d\alpha_1/d\chi_1 = 0$. The second relation implies that when $d\delta_1/d\chi_1$ (and hence, $d\alpha_1/d\chi_1$) is zero, $d^2\delta_1/d\chi_1^2$ and $d^2\alpha_1/d\chi_1^2 < 0$ have the same sign.

The width of the cusp-shaped region always increases as one moves away from the cusp point (Fig. 10a). To see this, observe that the above equations imply that

$$\frac{d\delta_1^2}{d\alpha_1} = \frac{\chi_1}{(1 + \chi_1)^2}$$

is an increasing function of χ_1. Hence, the slope at any point on the upper branch of the bifurcation curve is always greater than the slope of any point on the lower branch.

Appendix D: Bifurcation diagram for growth on lactose + glucose

In this case, the steady states satisfy the equations

$$\rho_1 = (\epsilon_1 + \alpha\epsilon_2)\epsilon_1, \qquad \rho_1 \equiv \frac{1}{1 + \alpha_1/(1 + \delta_1\epsilon_1)^2 + \hat{\alpha}_1/(1 + \delta_1\epsilon_1)^4}, \qquad \text{(D.1)}$$

$$\rho_2 = (\epsilon_1 + \alpha\epsilon_2)\epsilon_2, \qquad \rho_2 \equiv \frac{\alpha}{1 + \alpha_2/(1 + \delta_2\epsilon_2)}, \qquad \text{(D.2)}$$

where $\alpha = \beta\delta_1/\delta_2$. If a steady state corresponds to a fold bifurcation point, the determinant of the Jacobian,

$$J = \begin{bmatrix} \frac{2\alpha_1\delta_1/(1+\delta_1\epsilon_1)^3 + 4\hat{\alpha}_1\delta_1/(1+\delta_1\epsilon_1)^5}{\{1+\alpha_1/(1+\delta_1\epsilon_1)^2 + \hat{\alpha}_1/(1+\delta_1\epsilon_1)^4\}^2} - 2\epsilon_1 - \alpha\epsilon_2 & -\alpha\epsilon_1 \\ -\epsilon_2 & \frac{\alpha}{\{1+\alpha_2/(1+\delta_2\epsilon_2)\}^2}\frac{\alpha_2\delta_2}{(1+\delta_2\epsilon_2)^2} - \epsilon_1 - 2\alpha\epsilon_2 \end{bmatrix},$$

at that steady state must also be zero. Now, it follows from (D.1) that at a steady state

$$J_{11} = (\epsilon_1 + \alpha\epsilon_2)\epsilon_1\frac{2\alpha_1\delta_1/(1 + \delta_1\epsilon_1)^3 + 4\hat{\alpha}_1\delta_1/(1 + \delta_1\epsilon_1)^5}{1 + \alpha_1/(1 + \delta_1\epsilon_1)^2 + \hat{\alpha}_1/(1 + \delta_1\epsilon_1)^4} - 2\epsilon_1 - \alpha\epsilon_2$$

$$= (\epsilon_1 + \alpha\epsilon_2)p - \epsilon_1,$$

where

$$p \equiv 2 \frac{\delta_1 \epsilon_1}{1 + \delta_1 \epsilon_1} \frac{\alpha_1/(1 + \delta_1 \epsilon_1)^2 + 2\hat{\alpha}_1/(1 + \delta_1 \epsilon_1)^4}{1 + \alpha_1/(1 + \delta_1 \epsilon_1)^2 + \hat{\alpha}_1/(1 + \delta_1 \epsilon_1)^4} - 1.$$

Similarly, (D.2) implies that at a steady state

$$J_{22} = (\epsilon_1 + \alpha \epsilon_2) \epsilon_2 \frac{1}{1 + \alpha_2/(1 + \delta_2 \epsilon_2)} \frac{2}{(1 + \delta_2 \epsilon_2)^2} - \epsilon_1 - 2\alpha \epsilon_2,$$

$$= (\epsilon_1 + \alpha \epsilon_2)q - \alpha \epsilon_2$$

where

$$q \equiv \frac{\alpha_2}{\alpha_2 + (1 + \delta_2 \epsilon_2)} \frac{\delta_2 \epsilon_2}{1 + \delta_2 \epsilon_2} - 1.$$

It follows that $\det J$ is zero at a steady state if and only if

$$(\epsilon_1 + \alpha \epsilon_2)\left[(\epsilon_1 + \alpha \epsilon_2)pq - \alpha p \epsilon_2 - q\epsilon_1\right] = 0,$$

i.e.,

$$\alpha = \frac{\epsilon_1}{\epsilon_2}h, \quad h \equiv \frac{1/p - 1}{1 - 1/q}. \tag{D.3}$$

The bifurcation points satisfy Eqs. (D.1)–(D.3).

To determine the parametric representation of the bifurcation points, observe that (D.1), (D.2) yield $\epsilon_1/\epsilon_2 = \rho_1/\rho_2$, which can be substituted in (D.3) to obtain $\alpha = (\rho_1/\rho_2)h$, i.e.,

$$\alpha = \frac{\beta \delta_1}{\delta_2} = \sqrt{\frac{1 + \alpha_2/(1 + \chi_2)}{1 + \alpha_1/(1 + \chi_1)^2 + \hat{\alpha}_1/(1 + \chi_1)^4}} \sqrt{h}, \tag{D.4}$$

where h is now a function of χ_1 and χ_2. Eqs. (D.1), (D.2) also imply that

$$\rho_1 - \alpha \rho_2 = \epsilon_1^2 \left[1 - \alpha^2 \left(\frac{\epsilon_2}{\epsilon_1}\right)^2\right] = \epsilon_1^2 \left[1 - \alpha^2 \left(\frac{\rho_2}{\rho_1}\right)^2\right],$$
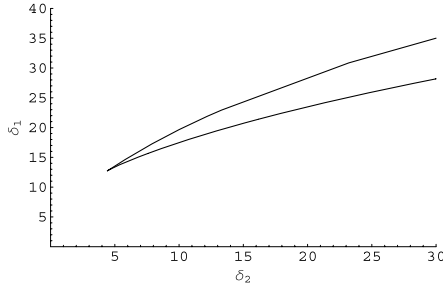
whence

$$\epsilon_1^2 = \rho_1 \frac{1}{1 + \alpha(\rho_2/\rho_1)} = \rho_1 \frac{1}{1 + h}.$$

Hence

$$\epsilon_1 = \sqrt{\frac{1}{1 + \alpha_1/(1 + \chi_1)^2 + \hat{\alpha}_1/(1 + \chi_1)^4}} \sqrt{\frac{1}{1 + h}},$$

and

$$\delta_1(\chi_1, \chi_2) = \frac{\chi_1}{\epsilon_1} = \chi_1 \sqrt{1 + \alpha_1/(1 + \chi_1)^2 + \hat{\alpha}_1/(1 + \chi_1)^4} \sqrt{1 + h}. \tag{D.5}$$

Fig. D.1 The bifurcation diagram for growth on glucose and lactose at $\alpha_1 = 170$, $\hat{\alpha}_1 = 0$, $\alpha_2 = 4$, $\beta = 1$. The δ_2-coordinate of the bifurcation curve is always positive, i.e., bistability is infeasible at sufficiently small δ_2. This reflects the fact that if the repression due to DNA looping is small, bistability is impossible during growth on pure lactose ($\delta_2 = 0$).

Finally,

$$\epsilon_2 = \frac{\rho_2}{\rho_1}\epsilon_1 = \frac{\alpha\sqrt{1 + \alpha_1/(1 + \chi_1)^2 + \hat{\alpha}_1/(1 + \chi_1)^4}}{1 + \alpha_2/(1 + \chi_2)}\sqrt{\frac{1}{1 + h}}.$$

It follows from (D.4) that

$$\epsilon_2 = \frac{1}{\sqrt{1 + \alpha_2/(1 + \chi_2)}}\sqrt{\frac{h}{1 + h}},$$

and

$$\delta_2(\chi_1, \chi_2) = \frac{\chi_2}{\epsilon_2} = \chi_2\sqrt{1 + \alpha_2/(1 + \chi_2)}\sqrt{\frac{1 + h}{h}}. \tag{D.6}$$

Substituting (D.5), (D.6) in (D.4) yields

$$\beta = \frac{\chi_1}{\chi_2}h \quad \Leftrightarrow \quad \beta\chi_2\frac{\alpha_2(\chi_2 + 2) + 2(1 + \chi_2)^2}{\alpha_2 + (1 + \chi_2)^2} = \frac{1}{p(\chi_1)} - 1. \tag{D.7}$$

Equations (D.5)–(D.7) provide a parametric representation of the bifurcation points.

Bistability is feasible if and only if and only if $0 < p < 1$ for some $\chi_1 > 0$. To see this, observe that the LHS of (D.7) is a monotonically increasing function of χ_2 for all $\chi_2 \geq 0$, and the RHS of (D.7) is positive if and only if $0 < p < 1$. It follows that for every $\chi_1 > 0$ such that $0 < p(\chi_1) < 1$, there is a unique $\chi_2 > 0$ satisfying (D.7). These pairs, $\chi_1, \chi_2 > 0$, define a curve on the $\chi_1\chi_2$-plane, and the variation of $\delta_1(\chi_1, \chi_2)$ and $\delta_2(\chi_1, \chi_2)$ along this curve delineates the bistable region on the $\delta_1\delta_2$-plane. In contrast, for every $\chi_1 > 0$ such that $p(\chi_1) < 0$ or $p(\chi_1) > 1$, the RHS of (D.7) is negative. Hence, there is no $\chi_2 > 0$ satisfying (D.7), and no bistability.

The condition, $p > 0$ for some $\chi_1 > 0$, is satisfied if and only if α_1 and $\hat{\alpha}_1$ lie above the full curve shown in Fig. 11. To see this, observe that p has a maximum on $\chi_1 > 0$ since $p(0) = -1$, $p(\infty) = -1$, and $p(\chi_1) > -1$ for $0 < \chi_1 < \infty$. The value of α_1 and $\hat{\alpha}_1$

at which a maximum of p touches the χ_1-axis satisfies the equations

$$p(\chi_1) = 0 \quad \Leftrightarrow \quad (\chi_1 - 1)\frac{\alpha_1}{(1 + \chi_1)^2} + (3\chi_1 - 1)\frac{\hat{\alpha}_1}{(1 + \chi_1)^2} = 1 + \chi_1,$$

$$p_{\chi_1}(\chi_1) = 0 \quad \Leftrightarrow \quad (3 - \chi_1)\frac{\alpha_1}{(1 + \chi_1)^2} + (7 - 9\chi_1)\frac{\hat{\alpha}_1}{(1 + \chi_1)^2} = 1 + \chi_1,$$

which can be solved to obtain

$$\alpha_1(\chi_1) = 2\frac{(1 + \chi_1)^3(3\chi_1 - 2)}{3\chi_1^2 - 3\chi_1 + 2}, \qquad \hat{\alpha}_1(\chi_1) = \frac{(1 + \chi_1)^5(2 - \chi_1)}{3\chi_1^2 - 3\chi_1 + 2}.$$

The above relations define the full curve shown in Fig. 11. Evidently, the $\hat{\alpha}_1$- and α_1-intercepts of the curve are 27 and $(5/3)^5$, respectively. Moreover, since $\partial p/\partial\hat{\alpha}_1 > 0$ for all $\chi_1 > 0$, the condition, $0 < p$ for some $\chi_1 > 0$, is satisfied precisely when α_1 and $\hat{\alpha}_1$ lie above this curve.

If α_1 and $\hat{\alpha}_1$ lie above the full curve in Fig. 11, there is an interval, say, $(\underline{\chi}_1, \overline{\chi}_1)$, on which $p > 0$. But there are two possibilities. Either p never exceeds 1 on this interval, or it exceeds 1 on some subinterval of $(\underline{\chi}_1, \overline{\chi}_1)$, say, $(\chi_{1,l}, \chi_{1,u})$. In the first case, the χ_2-coordinate of the curve defined by (D.7), and hence, the δ_2-coordinate of the bifurcation curve is always positive, i.e., the bifurcation diagram has the form shown in Fig. 12. In the second case, the χ_2-coordinate of the curve defined by (D.7) is zero at $\chi_1 = \chi_{1,l}, \chi_{1,u}$, and the δ_2-coordinate of the bifurcation curve is zero at the corresponding point. The bifurcation diagram, therefore, has the form shown in Fig. 12a.

One can check (by the method similar to the one shown above) that p exceeds 1 for some $\chi_1 > 0$ if and only α_1 and $\hat{\alpha}_1$ lie above the curve defined by the relations

$$\alpha_1(\chi_1) = 2\frac{(1 + \chi_1)^3(2\chi_1 - 3)}{3 - \chi_1}, \qquad \hat{\alpha}_1(\chi_1) = 3\frac{(1 + \chi_1)^5}{3 - \chi_1},$$

which is shown as the dashed curve in Fig. 11. Evidently, the $\hat{\alpha}_1$- intercept of the curve is $5^5/2^4$.

References

Babloyantz, A., Sanglier, M., 1972. Chemical instabilities of "all-or-none" type in β-galactosidase induction and active transport. FEBS Lett. 23, 364–366.

Benzer, S., 1953. Induced synthesis of enzymes in bacteria analyzed at the cellular level. Biochem. Biophys. Acta 11, 383–395.

Bettenbrock, K., Fischer, S., Kremling, A., Jahreis, K., Sauter, T., Gilles, E.-D., 2006. A quantitative approach to catabolite repression in *Escherichia coli*. J. Biol. Chem. 281(5), 2578–2584.

Chung, J.D., Stephanopoulos, G., 1996. On physiological multiplicity and population heterogeneity of biological systems. Chem. Eng. Sci. 51, 1509–1521.

Cohn, M., Horibata, K., 1959a. Analysis of the differentiation and of the heterogeneity within a population of *Escherichia coli* undergoing induced β-galactoside synthesis. J. Bacteriol. 78, 613–623.

Cohn, M., Horibata, K., 1959b. Inhibition by glucose of the induced synthesis of the β-galactoside-enzyme system of *Escherichia coli*. Analysis of maintenance. J. Bacteriol. 78, 601–612.

Herzenberg, L.A., 1959. Studies on the induction of β-galactosidase in a cryptic strain of *Escherichia coli*. Biochim. Biophys. Acta 31(2), 525–538.

Kepes, A., 1960. Kinetic studies on galactoside permease of *Escherichia coli*. Biochim. Biophys. Acta 40, 70–84.

Kuhlman, T., Zhang, Z., Saier, M.H., Hwa, T., 2007. Combinatorial transcriptional control of the lactose operon of *Escherichia coli*. Proc. Natl. Acad. Sci. U.S.A. 104(14), 6043–6048.

Laurent, M., Charvin, G., Guespin-Michel, J., 2005. Bistability and hysteresis in epigenetic regulation of the lactose operon. Since Delbrück, a long series of ignored models. Cell. Mol. Biol. (Noisy-le-grand) 51(7), 583–594.

Lewis, M., 2005. The *lac* repressor. C. R. Biol. 328(6), 521–548.

Loomis, W.F., Magasanik, B., 1967. Glucose-lactose diauxie in *Escherichia coli*. J. Bacteriol. 93(4), 1397–1401.

Mahaffy, J.M., Savev, E.S., 1999. Stability analysis for a mathematical model of the *lac* operon. Q. Appl. Math. 57, 37–53.

Monod, J., 1947. The phenomenon of enzymatic adaptation and its bearings on problems of genetics and cellular differentiation. Growth 11, 223–289.

Narang, A., 2007. Effect of DNA looping on the induction kinetics of the *lac* operon. J. Theor. Biol. 247, 695–712.

Narang, A., Pilyugin, S.S., 2007. Bacterial gene regulation in diauxic and nondiauxic growth. J. Theor. Biol. 244, 326–348.

Oehler, S., Amouyal, M., Kolkhof, P., von Wilcken-Bergmann, B., Müller-Hill, B., 1994. Quality and position of the three *lac* operators of *E. coli* define efficiency of repression. EMBO J. 13(14), 3348–3355.

Oehler, S., Eismann, E.R., Krämer, H., Müller-Hill, B., 1990. The three operators of the *lac* operon cooperate in repression. EMBO J. 9(4), 973–979.

Oehler, S., Alberti, S., Müller-Hill, B., 2006. Induction of the *lac* promoter in the absence of DNA loops and the stoichiometry of induction. Nucleic Acids Res. 34(2), 606–612.

Ozbudak, E.M., Thattai, M., Lim, H.N., Shraiman, B.I., van Oudenaarden, A., 2004. Multistability in the lactose utilization network of *Escherichia coli*. Nature 427, 737–740.

Plumbridge, J., 2003. Regulation of gene expression in the PTS in *Escherichia coli*: the role and interactions of Mlc. Curr. Opin. Microbiol. 5, 187–193.

Santillán, M., Mackey, M.C., Zeron, E.S., 2007. Origin of bistability in the *lac* operon. Biophys. J. 92(11), 3830–3842.

Savageau, M.A., 2001. Design principles for elementary gene circuits: elements, methods, and examples. Chaos 11(1), 142–159.

Spiegelman, S., 1948. Differentiation as the controlled production of unique enzymatic patterns. In: Danielli, J.F., Brown, R. (Eds.), Growth in Relation to Differentiation and Morphogenesis. Symposium of the Society for Experimental Biology, vol. II, pp. 286–325. Academic, San Diego.

Tempest, D.W., Herbert, D., Phipps, P.J., 1967. Studies on the growth of *Aerobacter aerogenes* at low dilution rates in a chemostat. In: Microbial Physiology and Continuous Culture, pp. 240–253. HMSO, London.

van Hoek, M.J.A., Hogeweg, P., 2006. *In silico* evolved *lac* operons exhibit bistability for artificial inducers, but not for lactose. Biophys. J. 91(8), 2833–2843.

Yagil, G., Yagil, E., 1971. On the relation between effector concentration and the rate of induced enzyme synthesis. Biophys. J. 11, 11–27.